

**NASA CONTRACTOR
REPORT**



NASA CR-25

0061235

TECH LIBRARY KAFB, NM



LOAN COPY: RETURN TO
AFWL TECHNICAL LIBRARY
KIRTLAND AFB, N. M.

2. u/u

NASA CR-2549

**DESIGN AND FABRICATION
OF COMPOSITE WING PANELS
CONTAINING A PRODUCTION SPLICE**

D. L. Reed

Prepared by

GENERAL DYNAMICS / FORT WORTH


Fort Worth, Texas

for Langley Research Center



NATIONAL AERONAUTICS AND SPACE ADMINISTRATION • WASHINGTON, D. C. • AUGUST 1975

5.

1. Report No. NASA CR-2549		2. Government Accession No.		 0061235 AUGUST 1975	
4. Title and Subtitle DESIGN AND FABRICATION OF COMPOSITE WING PANELS CONTAINING A PRODUCTION SPLICE				6. Performing Organization Code	
				8. Performing Organization Report No.	
7. Author(s) D. L. REED				10. Work Unit No.	
9. Performing Organization Name and Address GENERAL DYNAMICS CORPORATION FORT WORTH DIVISION FORT WORTH, TEXAS				11. Contract or Grant No. NAS1-11974	
				13. Type of Report and Period Covered CONTRACTOR REPORT	
12. Sponsoring Agency Name and Address NATIONAL AERONAUTICS AND SPACE ADMINISTRATION WASHINGTON, D.C. 20546				14. Sponsoring Agency Code	
15. Supplementary Notes THIS IS A TOPICAL REPORT					
16. Abstract <p>BOLTED SPECIMENS REPRESENTATIVE OF BOTH UPPER AND LOWER WING SURFACE SPLICES OF A TRANSPORT AIRCRAFT WERE DESIGNED AND MANUFACTURED FOR STATIC AND RANDOM LOAD TENSION AND COMPRESSION FATIGUE TESTING INCLUDING GROUND-AIR-GROUND LOAD REVERSALS. THE SPECIMENS WERE FABRICATED WITH GRAPHITE-EPOXY COMPOSITE MATERIAL. MULTIPLE TESTS WERE CONDUCTED AT VARIOUS LOAD LEVELS AND THE RESULTS WERE USED AS INPUT TO A STATISTICAL WEAROUT MODEL. THE STATICALLY DESIGNED SPECIMENS PERFORMED VERY WELL UNDER HIGHLY MAGNIFIED FATIGUE LOADINGS. TWO LARGE PANELS, ONE TENSION AND COMPRESSION, WERE FABRICATED FOR TESTING BY NASA-LRC.</p>					
17. Key Words (Suggested by Author(s)) COMPOSITE MATERIALS; BOLTED JOINTS; STRENGTH; FATIGUE; TENSION AND COMPRESSION; RELIABILITY; RANDOM LOADS			18. Distribution Statement UNCLASSIFIED - UNLIMITED Subject Category 39 - Structural Mechanics		
19. Security Classif. (of this report) UNCLASSIFIED		20. Security Classif. (of this page) UNCLASSIFIED		21. No. of Pages 79	
				22. Price* \$4.75	

CONTENTS

<u>Section</u>		<u>Page</u>
1.0	SUMMARY.....	1
2.0	INTRODUCTION.....	2
3.0	DEVELOPMENT TEST PROGRAM.....	3
3.1	Specimen Design.....	3
3.1.1	Design Loads.....	3
3.1.2	Design Concept.....	4
3.1.3	Material.....	4
3.1.4	Splice Design Method.....	8
3.1.5	Splice Test Specimens.....	12
3.1.6	Skin Specimens.....	12
3.2	Specimen Fabrication.....	15
3.2.1	Nondestructive Testing.....	16
3.3	Fatigue Spectrum Generation.....	16
3.4	Laboratory Test Equipment.....	22
3.4.1	Load Control System.....	22
3.4.2	Test Fixtures.....	22
3.5	Static Test Results for Joints.....	27
3.5.1	End Grip Problems.....	27
3.5.2	Tension.....	30
3.5.3	Compression.....	34
3.6	Fatigue Test Results for Joints.....	34
3.6.1	Magnified Spectra.....	37
3.6.2	Real Spectrum.....	46
3.6.3	Wearout Model.....	46
3.7	Static and Fatigue Test Results for Skin Specimens.....	51
3.8	Discussions.....	53

CONTENTS (Continued)

<u>Section</u>		<u>Page</u>
4.0	LARGE PANEL DESIGN AND FABRICATION.....	55
	4.1 Panel Design.....	55
	4.2 Panel Fabrication.....	61
5.0	CONCLUSIONS AND RECOMMENDATIONS.....	71
	5.1 Conclusions.....	71
	5.2 Recommendations.....	71
6.0	REFERENCES.....	73

FIGURES

<u>Figure</u>		<u>Page</u>
1	Basic Splice Concept.....	5
2	Joint Specimen.....	6
3	Tension Splice Design.....	10
4	Compression Splice Design.....	11
5	Detail Design of Compression Splice Specimens	13
6	Detail Design of Tension Splice Specimens....	14
7	Tension and Compression Joint Specimens.....	17
8	Transport Load Spectrum.....	18
9	Mapping Function.....	20
10	Comparison of Input and Output Spectra.....	21
11	One Flight of Random Load History.....	23
12	Schematic of Closed Loop Test Equipment.....	24
13	Load Control System.....	25
14	Test Fixture.....	26
15	Compression Specimen Under Compression Load..	28
16	Compression Specimen Under Tension Load.....	28
17	Static Compression Specimen End Grip Failure.	29
18	Static Tension Specimen End Grip Failure.....	29
19	Typical Load-Displacement Curve for Tension Splice Specimen.....	31
20	Static Tension Failure.....	32
21	Typical Load-Displacement Curve for Compres- sion Splice Specimen.....	35

FIGURES (Continued)

<u>Figure</u>		<u>Page</u>
22	Splitting Failure Mode in Static Compression Specimen.....	36
23	Spectrum Magnification Effects.....	40
24	Tension Fatigue Failure at 0.465 Lifetimes...	41
25	Tension Fatigue Damage at 0.854 Lifetimes....	42
26	Tension Fatigue Failure at 0.862 Lifetimes...	43
27	Tension Splice Damage at 4.010 Lifetimes.....	45
28	Wing Splice Tension Joint Data.....	48
29	Wing Splice Compression Joint Data.....	49
30	Sandwich Skin Specimens.....	52
31	Upper Panel Design.....	57
32	Upper Panel Design (Sheet 2).....	58
33	Lower Panel Design.....	59
34	Lower Panel Design (Sheet 2).....	60
35	Layup Showing Core Detail.....	62
36	Completed Layup Before Cure.....	64
37	Large Panel and Specimens Cut From Blank.....	65
38	Completed Test Specimens.....	66
39	Tension Splice Panel - Outer Surface.....	67
40	Tension Splice Panel - Inner Surface.....	68
41	Compression Splice Panel - Outer Surface.....	69
42	Compression Splice Panel - Inner Surface.....	70

DESIGN AND FABRICATION OF
COMPOSITE WING PANELS
CONTAINING A PRODUCTION
SPLICE

by

D. L. REED

General Dynamics Corporation
Fort Worth Division

1.0 SUMMARY

Joints for both the upper and lower wing surfaces were designed for a major splice in a graphite-epoxy wing of a transport. The upper and lower surface joints were designed for representative compression and tension loadings respectively and a 60,000 hour fatigue life. A single scarf, bolted joint capable of assembly and disassembly was selected for both upper and lower splices. The solid laminate of the joints was blended into a honeycomb sandwich of the same thickness.

Test specimens representing a section of the joints with a single line of bolts were fabricated and tested to verify that the design satisfied the strength and life requirements. The fatigue tests were conducted with a random flight-by-flight load history. The static tension and compression strengths of the specimens were nearly identical to the design strengths. Except for fatigue failures of bolt heads, no fatigue damage occurred in 10 lifetimes of fatigue loading. Residual strengths after the fatigue loading were essentially equal to the original static strengths.

Two large honeycomb panels containing the joints (one for the upper surface and one for the lower) were fabricated for testing at NASA-Langley Research Center. The design of these panels was based on the test results for the joint specimens with the single line of bolts.

2.0 INTRODUCTION

The objective of this program was to design and fabricate an upper and lower wing panel containing chordwise splices for a next generation transport aircraft. The panels were to be made of composite materials and represent production splices capable of disassembly and reassembly. These panels were to be designed for both static loading and a service fatigue life of 60,000 flight hours. After these wing splice panels were designed and fabricated, they were to be delivered to NASA for fatigue testing at the Langley Research Center.

A development test program was initiated to design the wing splice panels. In this program static and fatigue tests were conducted on a representative element of the upper and lower splice panels. The development test program for these specimens is reported in Section 3.0.

The results of the development test program were used to design the large upper and lower wing panels containing the production splice. The design of these panels and the end grips for mating with the NASA test machine are reported in Section 4.0.

Section 5.0 contains a discussion of conclusions and recommendations.

3.0 DEVELOPMENT TEST PROGRAM

The development test program was initiated to generate design data for the large panel design and to uncover problems that might be encountered in fabricating the large wing panels. Because no well-established fatigue design methodology existed, the splice was designed first on a static basis. Then, static and fatigue tests were conducted on the statically designed joint specimens to scale the static designs to satisfy the required life. A joint specimen with a single line of bolts was chosen to represent a typical element of the large panels.

This section discusses the design of the development joint specimens, the fabrication of the specimens, the fatigue test spectrum, the testing system, the static test results, the fatigue test results, and a discussion of the results from the development test program.

3.1 SPECIMEN DESIGN

The design of the development test specimens involved the design loads and a material system as well as a design concept for the joints. Each of these items will now be discussed.

3.1.1 Design Loads

The static limit design loads for the upper surface (compression) splice panel were specified as 2.627 MN/m (15,000 pounds/inch) in compression and 1.051 MN/m (6,000 pounds/inch) in tension. The static limit design loads for the lower surface (tension) splice panel were specified as 2.627 MN/m (15,000 pounds/inch) in tension and 1.051 MN/m (6,000 pounds/inch) in compression. The static ultimate load factor was specified as 1.5 times the limit loads. Thus, the ultimate design loads were 3.940 MN/m (22,500 pounds/inch) in compression for the upper surface splice and 3.940 MN/m (22,500 pounds/inch) in tension for the lower surface splice. In order to reflect the torsional stiffness of the wing, the panels were also required to have a minimum shear stiffness of $Gt = 140.1 \text{ MN/m}$ (0.8×10^6 pounds/inch), where G is the effective shear modulus and t is the effective thickness of the panel.

The fatigue loading spectrum is discussed in a later section.

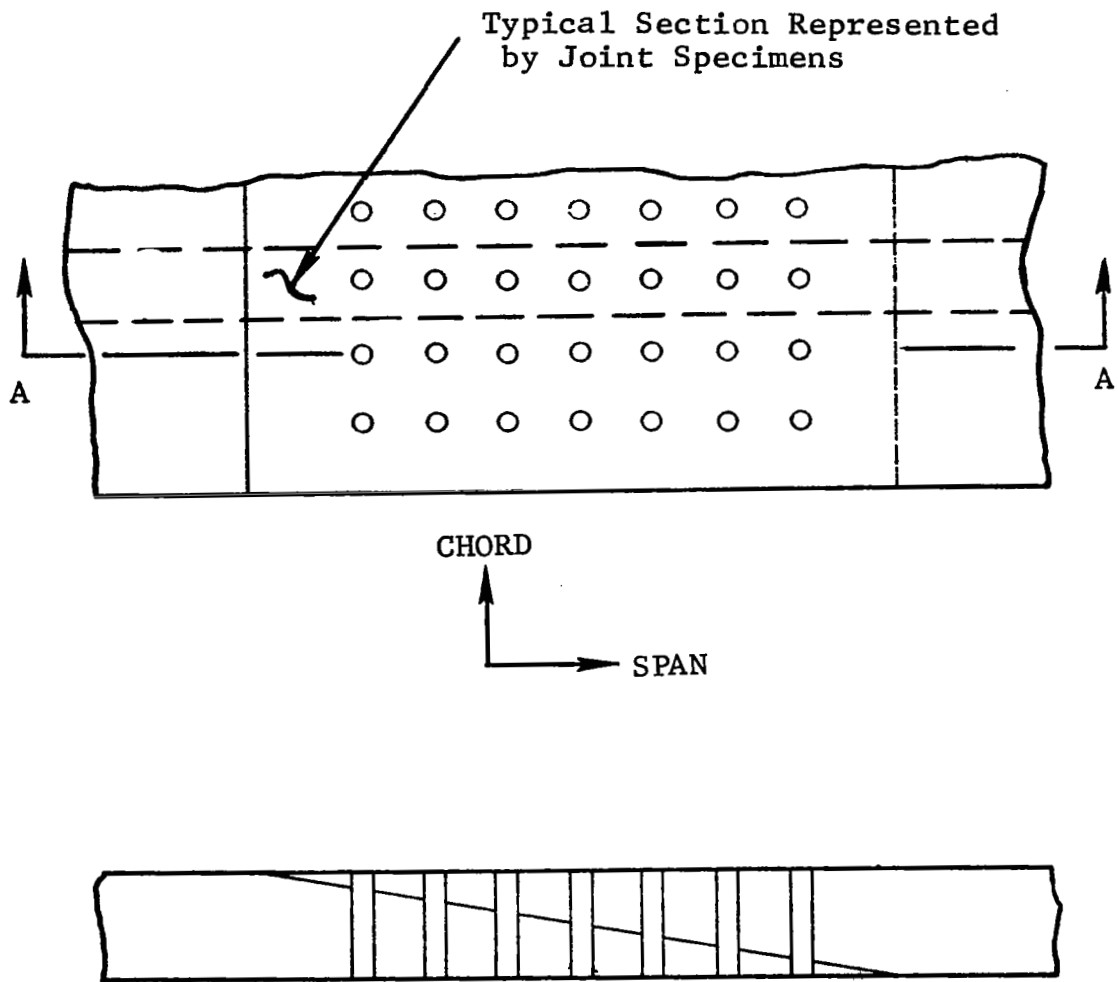
3.1.2 Design Concept

The basic design concept for the wing panel splice is shown in Figure 1. The mating pieces of the wing panel are joined at a machined scarf interface by mechanical fasteners, which are countersunk on the aerodynamic surface. The simplicity inherent in both analysis and fabrication of the basic splice makes this concept especially attractive. The solid laminate construction in the splice area can be blended into a honeycomb sandwich wing construction in the bays on either side of the splice bay. Figure 2 shows the joint specimen used in the development test program. The honeycomb sandwich was not included in the test section of the joint specimen because failure is not likely to occur in the sandwich. However, it was included in the ends of the specimen to develop the fabrication process for the transition from solid laminate to honeycomb sandwich and as a means of saving graphite material.

It should be noted that an optimum honeycomb sandwich for a wing surface would likely be thicker than that determined here by considering only the strength of the joint - especially the upper (compression) wing surface. Thus, these splice panels would likely have to be blended into a thicker sandwich panel in the adjacent wing bays. This transition could probably be made at the ribs adjacent to the bay containing the splice. Although the scope of the present program would not allow a detailed study of such a transition, the concept is feasible and is probably lighter than one where the thickness of the joint panel would be equal to that of the adjacent bay panels.

3.1.3 Material

Thornel 300/5208 graphite-epoxy (a product of Narmco Materials of Costa Mesa, California) was chosen for this program and was purchased in accordance with General Dynamics specification FMS-2023 Type III, Form C. Table I presents the basic lamina unidirectional data that was used in the design of the splice specimens. Acceptance tests were conducted on the graphite-epoxy material when it was received to assure that it met the minimum requirements of the specification. The design ultimate values presented in Table I represent averages over a large historical data sample and thus were used in the design.



Section A-A

Figure 1 Basic Splice Concept

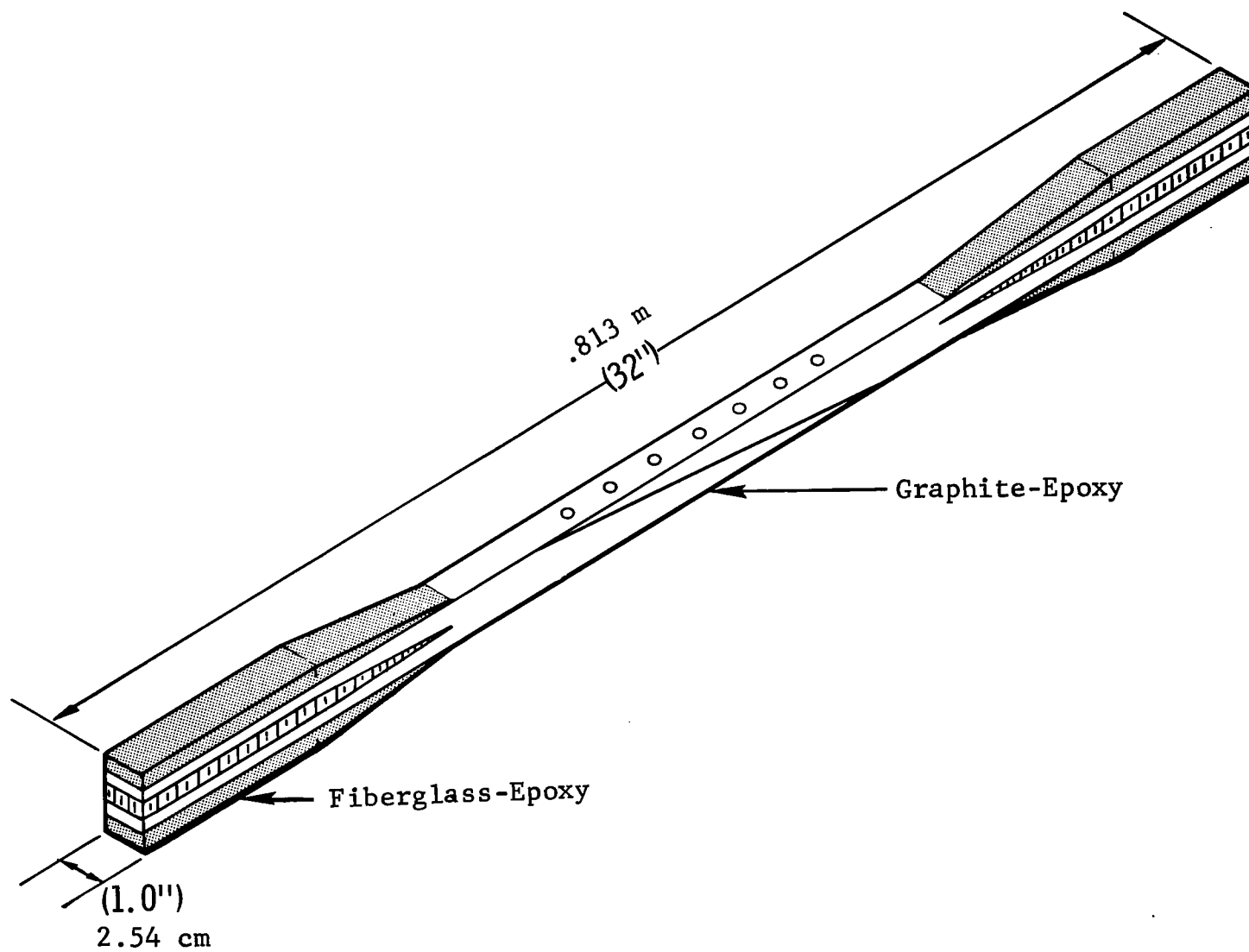


Figure 2 Joint Specimen

Table I LAMINA UNIDIRECTIONAL PROPERTIES FOR
THORNEL 300/5208 GRAPHITE MATERIAL

$$E_1 = 137.2 \text{ GPa } (19.9 \times 10^6 \text{ psi})$$

$$E_2 = 9.65 \text{ GPa } (1.4 \times 10^6 \text{ psi})$$

$$G_{12} = 4.48 \text{ GPa } (0.65 \times 10^6 \text{ psi})$$

$$\nu_{12} = 0.28$$

Strain
Average Ultimate

Tension

Longitudinal
Transverse

9.317 mm/m (9317 μ in./in.)
4.294 mm/m (4294 μ in./in.)

Compression

Longitudinal
Transverse

11.495 mm/m (11495 μ in./in.)
15.820 mm/m (15820 μ in./in.)

Shear

15.000 mm/m (15000 μ in./in.)

3.1.4 Splice Design Method

The initial assumption in the splice design was that all bolts transfer an equal amount of load. In most metal bolted joints, this is achieved only after yielding and a redistribution of load has taken place. However, with composites, it is possible to tailor the laminate in the joint to result in equal bolt loads. Strain matching techniques were used to assure equal bolt loads.

The strength design of the laminate at each bolt location was based on a fracture model. The applicability of classical fracture mechanics to the loaded or unloaded hole problem was developed in Reference 1 and justified in Reference 2. This model depends on a fracture hypothesis which states that a threshold volume of material must be stressed to a critical level before fracture develops. This threshold volume of material is characterized by the dimension "a" and is called an intense energy region in Reference 1. The dimension "a" is determined through tests of open and loaded holes. A typical bolted joint element (i.e. an element of the joint containing only one hole with a bearing load and a load being transferred past the hole in the plate) was obtained by superposition of an open hole (all load transferred past hole) and a loaded hole (all load in plate taken out at hole). A width correction factor is also part of the model. This bolted joint strength model had been programmed for a mini-computer and used to predict the failure strengths for both boron-epoxy and graphite-epoxy laminates. For a data sampling of 101 points containing open, loaded and combined loadings in boron-epoxy laminates, the average test failure divided by predicted failure was 1.000. In 65 graphite-epoxy laminates, the average test failure to predicted failure ratio was 1.075. These test points cover a range of hole diameters from 0.381 mm (0.015 inches) to 2.54 cm (1.00 inch) and a range of laminates from 0 to 70 percent 0-degree fiber content (Reference 2).

The design procedure for the tension splice began with using the strength model to obtain an optimum design for the laminates at the thin and thick ends of the scarf. An assumed number of bolts and the assumed equal bolt load distribution was used in doing this. Once the thickness of the scarf at these two locations had been determined, the overall splice thickness is simply the sum of these two numbers. The scarf angle is determined from the number of bolts along the splice, the previously determined thickness of the scarf at the thick

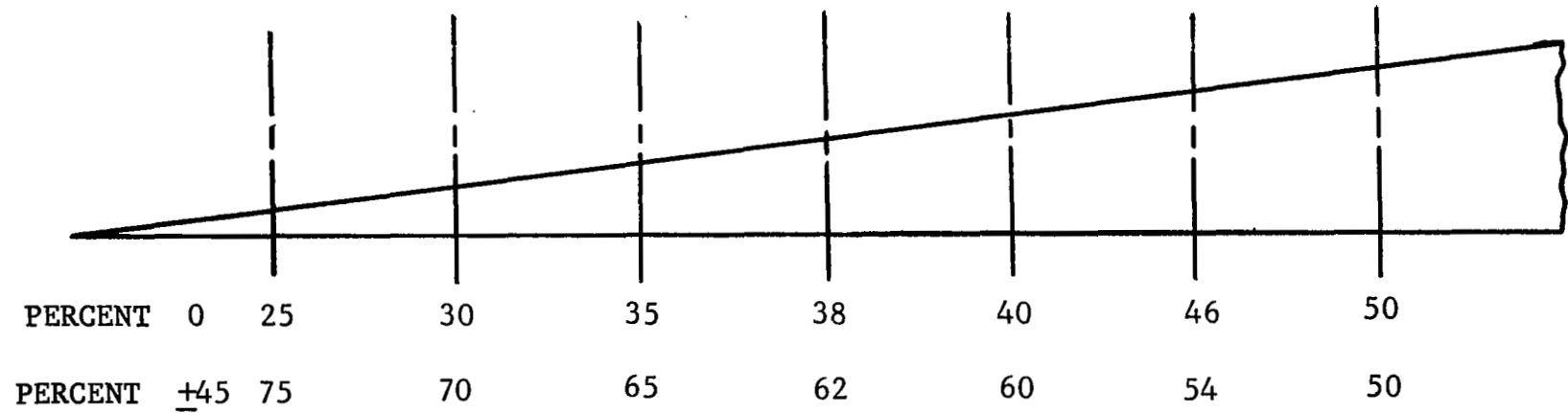
and thin end, and a bolt spacing of four times the bolt diameter. Several designs were evaluated; each had a different number of bolts (the minimum number of bolts is determined by the load to be transferred and the single shear capacity of the bolts). The design chosen for the tension splice was a seven-bolt configuration because of minimum weight considerations. As the splice region lengthens, the panel weight increases because of the solid laminate region.

The final step in the splice design was the determination of the laminate at each intermediate bolt location. The ideal situation from a manufacturing point of view would probably be a linear variation from the laminate modulus at the thin end of the scarf to the modulus at the thick end of the scarf. Using the criteria that the strain level be equal in the upper and lower parts of the splice (at the mid-point between each bolt), the laminate modulus (and therefore the ply orientations) was determined to approximate the linear variation. The criteria of equal strain in the upper and lower parts of the joint leads to the following relationship,

$$\frac{E_{Ui}}{E_{Li}} = \left(\frac{N-i}{i} \right) \frac{t_{Li}}{t_{Ui}}$$

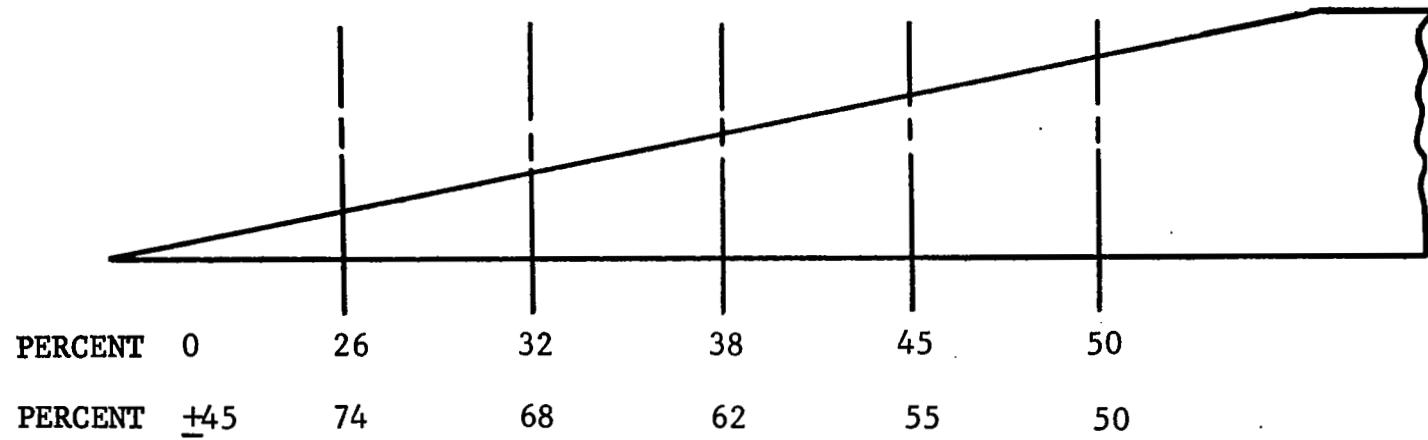
where, $i = i^{th}$ position between bolts, $N =$ number of bolts, E_{Ui} , E_{Li} = laminate modulus in the upper and lower parts at the i^{th} position, respectively, and t_{Ui} , t_{Li} = laminate thickness in the upper and lower parts at the i^{th} position, respectively. This relationship was used to determine the laminate moduli along the scarf. The equation was used in an iterative fashion to approach a linear variation in laminate modulus. The strength model was then used to see if an adequate margin was attained at each bolt location. In all cases the resulting margins were adequate and thus the design was completed. The tension splice design is shown in Figure 3.

The same design procedure (using the strength model) as that outlined above for the tension splice was used for the design of the compression splice. The compression splice design is shown in Figure 4. Because of compression buckling, the minimum number of five bolts (resulting in the thickest joint) was used in this design.



$t_{\text{TOTAL}} = 27.18\text{mm (1.07 inches)}$ 7 BOLTS - 6.35mm (0.25 inches)
 (195 layers)

Figure 3 Tension Splice Design



$t_{\text{TOTAL}} = 31.45\text{mm (1.238 inches)}$ 5 BOLTS - $6.35\text{mm (0.25 inches)}$
 (225 layers)

Figure 4 Compression Splice Design

3.1.5 Splice Test Specimens

The details of the compression and tension splice test specimens are shown in Figures 5 and 6, respectively. The design requirements for the full panels were a rib and spar spacing of 0.762 m (30 inches) and 1.473 m (58 inches), respectively. Since the splice region is the critical design portion of the test specimens and in an effort to reduce the amount of graphite material used in the specimens, the specimens were shortened for the development test program and do not represent one transport aircraft rib spacing in length. Fiberglass blocks (see Figures 5 and 6) were used in the end grip region to prevent crushing when the specimens were installed in the test fixtures.

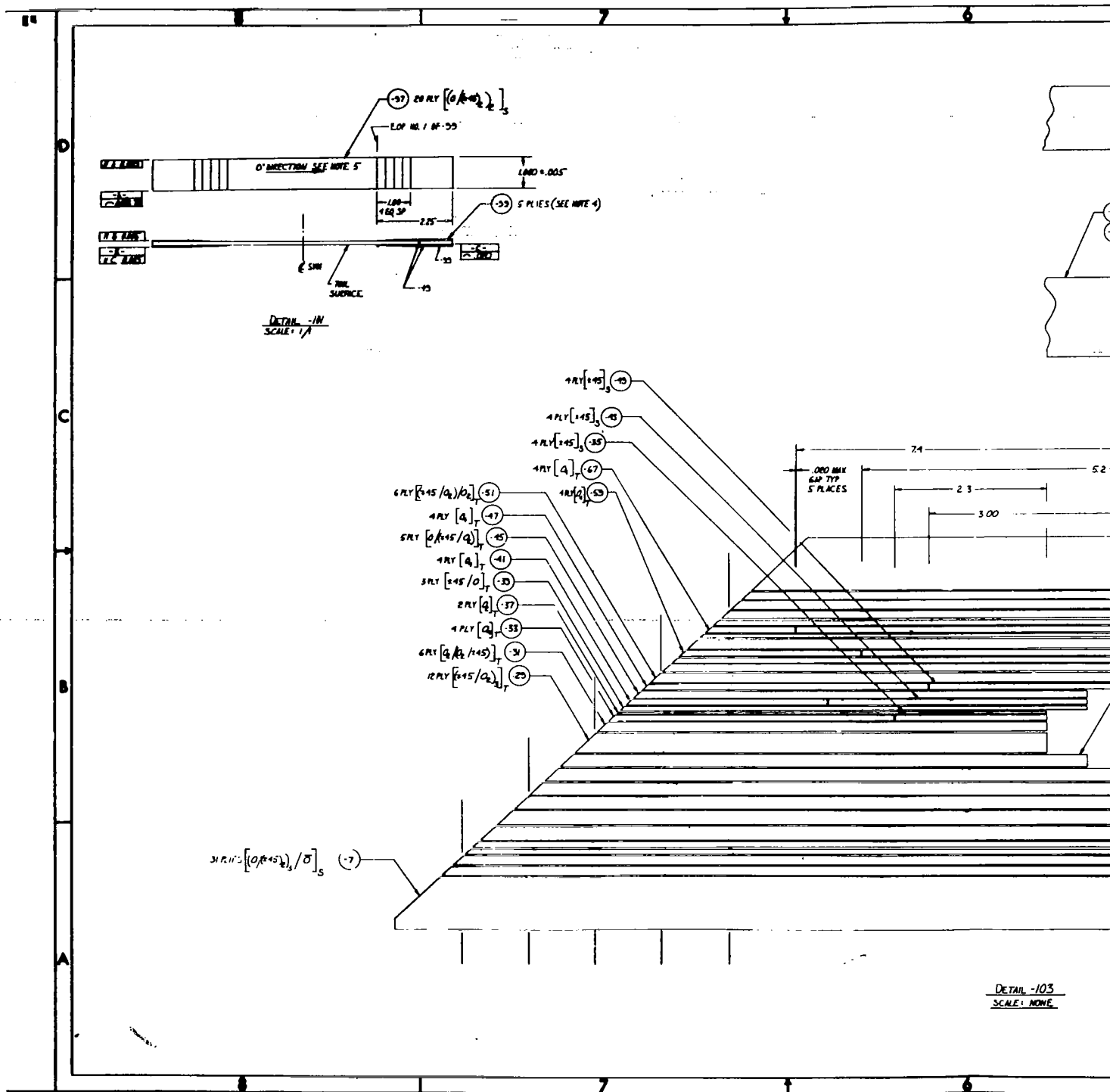
A buckling check of the compression development test specimen was made using the finite element program NASTRAN. Simulating the specimen as a pinned-end column, a buckling load of 87.198 kN (19603 pounds) or 0.871 times ultimate load was predicted for buckling in the thickness direction. Similarly, for a fixed end column, a buckling load of 512.164 kN (115,139 pounds) or 5.117 times ultimate load was predicted. Since the end fixity of the test apparatus was somewhat greater than the pinned-end condition, it was decided that no external restraints would be required to prevent buckling in the thickness direction mode.

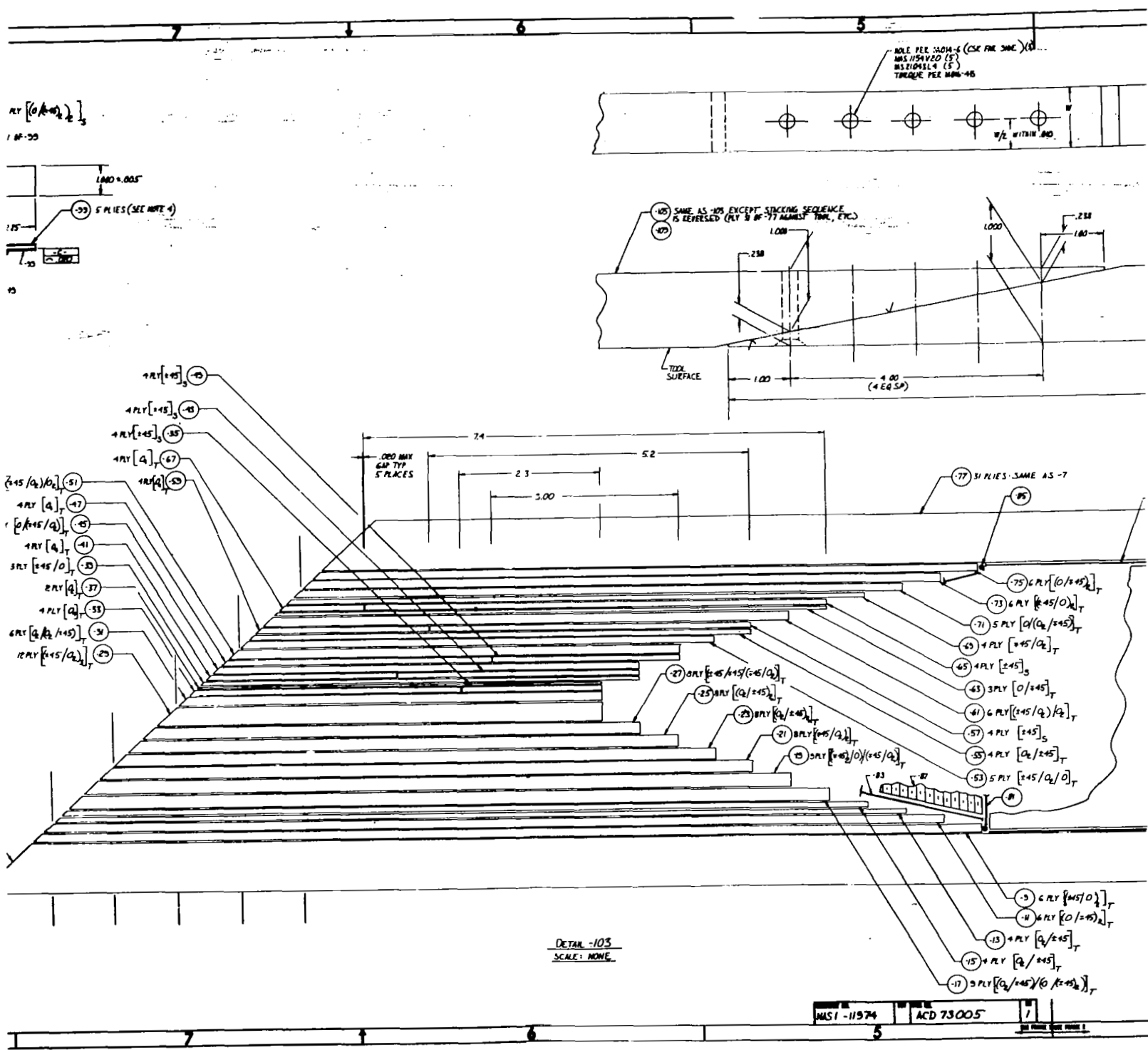
A buckling check was also made for side buckling of the test specimens. A buckling load of 50.830 kN (11,427 pounds) or 0.508 times ultimate load was predicted for a pinned-end column. Since this buckling load was so low, it was decided to use aluminum side plates to increase the side buckling load. With the side plates added to the simulation, a buckling load of 221.321 kN (49,755 pounds) or 2.211 times ultimate load was predicted.

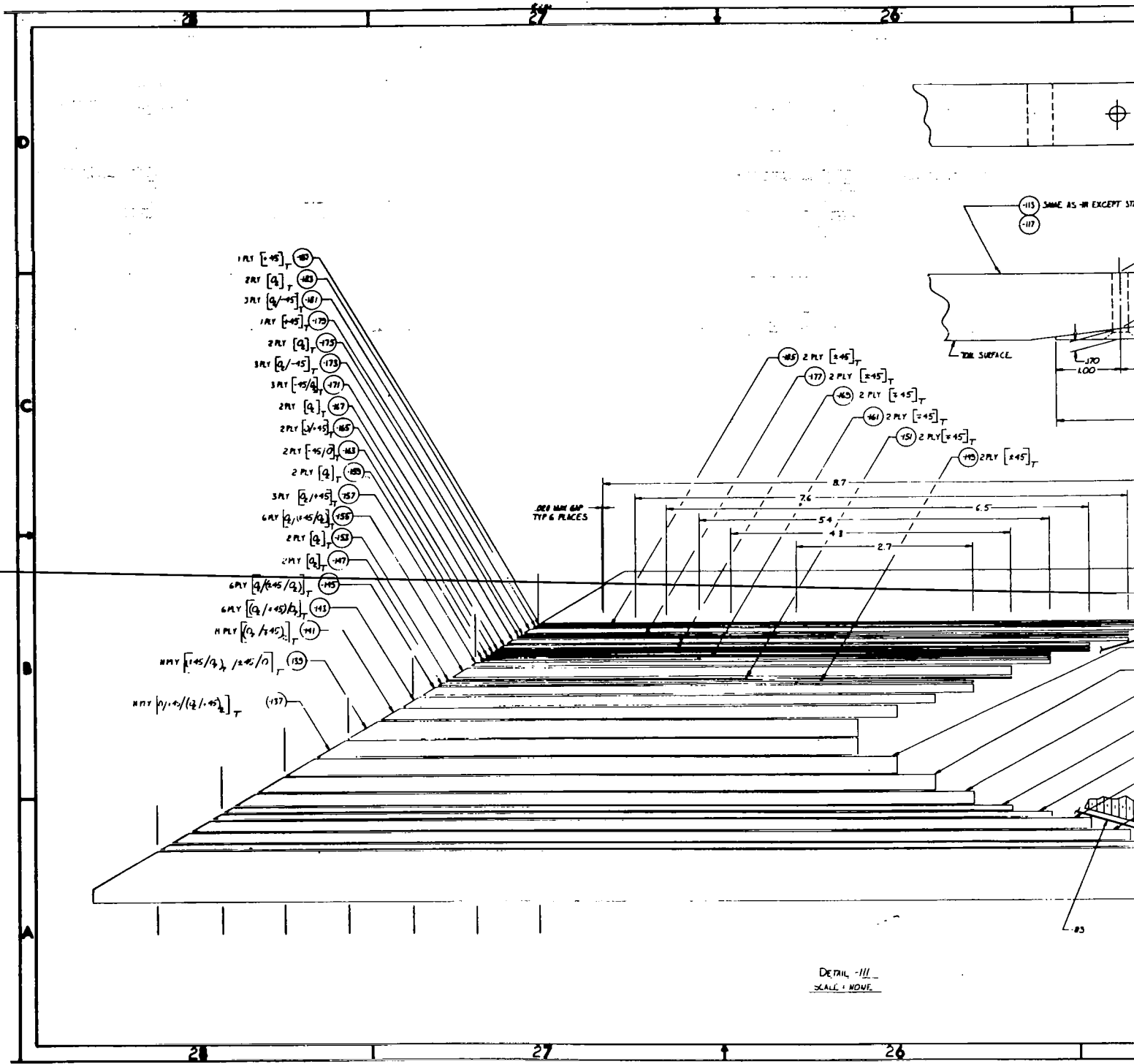
Twenty tension and twenty compression splice specimens were fabricated for static and fatigue testing.

3.1.6 Skin Specimens

Since the large splice panels will contain a sandwich construction section, test specimens representative of the skin laminate were fabricated. The details of these test specimens are shown in Figure 5. Twenty of these specimens were fabricated for static and fatigue testing.







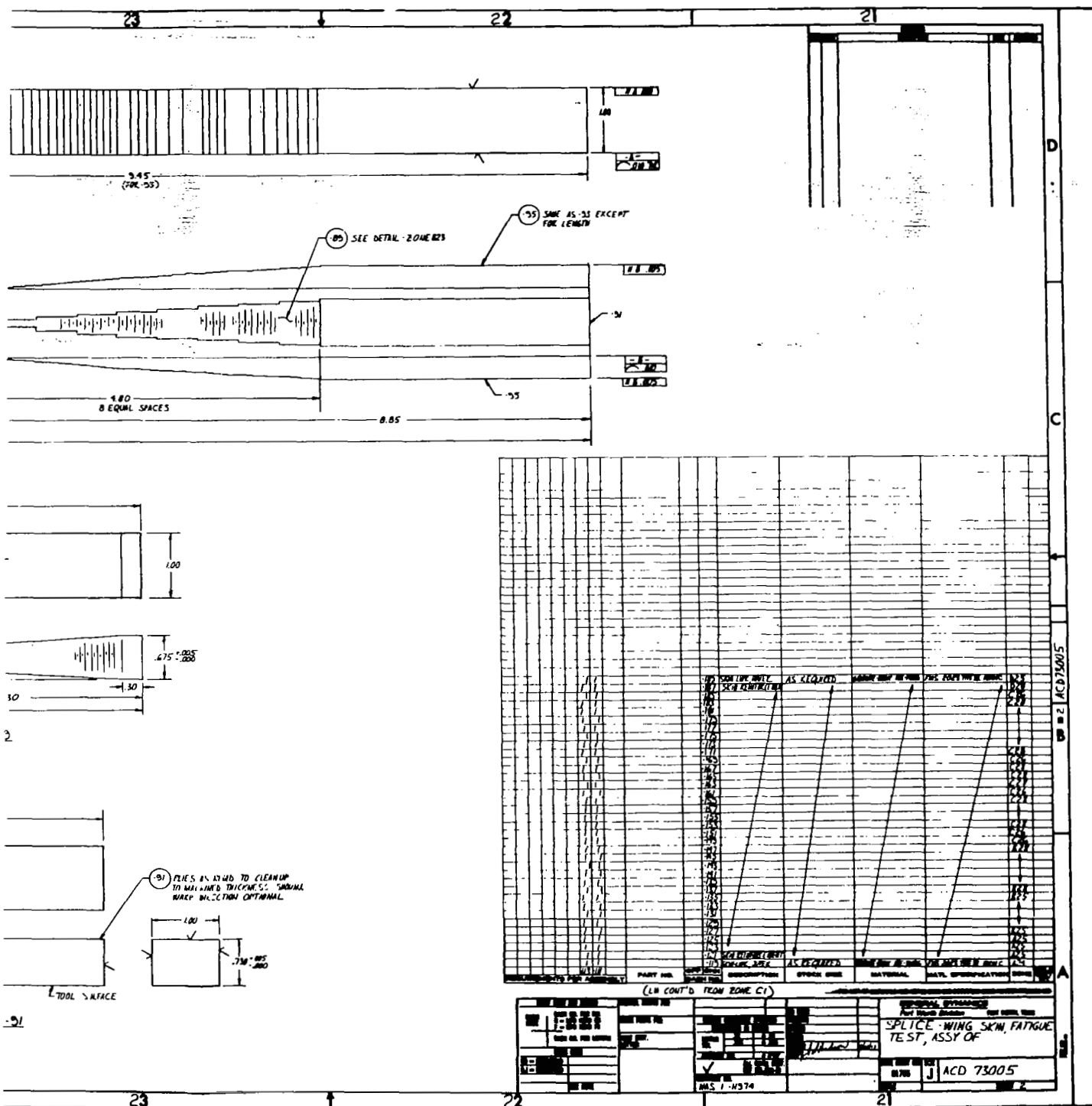


Figure 6 Detail Design of Tension Splice Specimen

3.2 SPECIMEN FABRICATION

The splice specimens were manufactured in wide panels (approximately 0.5588 m (22 inches)) and then cut into the 20 individual specimens (2.54 cm (one inch) wide). In order to reduce the amount of hand layup, the numerically controlled tape-laying machine was used to lay the sandwich skins and large sublaminates which recur throughout the joint. Then, these sublamine sheets were cut into the required sizes and hand laid, beginning with one surface and continuing to the other surface.

Because the laminates were different for each piece of the joint, the joint could not be laid-up as a continuous part and later be cut apart at the splice line. Thus, the sublamine sheets were butted together along the scarf angle. After the first half of the joint panel was reached, the core material and the precured fiberglass end blocks (see Figures 5 and 6) were added. Next, the top half of the joint panel was laid up and the entire panel cured in a single operation.

The tapered fiberglass end grips (see Figures 5 and 6) were laid up and cured separately and then were bonded to the previously cured large panel.

The wide panels were then sawed into the 2.54 cm (one inch) wide tension and compression splice specimens and, the sides of the specimens were machined smooth. Next, each specimen was cut apart along the scarf line, and the scarf surfaces were machined to make a good mating surface. The surfaces of the fiberglass end grips were also machined parallel to the specimen faces. Finally, the two halves of the specimens were clamped together, and the holes for the bolts were drilled, reamed, and countersunk one at a time. Hole clearances similar to what would be used for metal structure were used for these holes. After each hole was finished, a bolt was inserted to hold the specimen together while the remaining holes were being drilled.

A problem occurred during the fabrication of the tension splice specimens that required a repair. A sheet of mylar (used to lay the graphite on during the lay-up operation) was left in the laminate of one-half of the panel. After the panel had been sawed into the 2.54 cm (one inch) widths and the scarf angle had been cut, all the pieces from that half of the panel were found to delaminate at the mylar. The delamination extended

from the scarfed end back to the honeycomb core at a depth of about one-fourth the thickness.

In order to develop a repair procedure, a small panel with a layer of mylar in the laminate was fabricated and cut into several pieces. The delaminated surfaces were inspected and the mylar was found to have diffused into the graphite. Four of the pieces were then rebonded using two types of adhesives and two degrees of sanding. Clamps were used to apply pressure during the cure cycle. Horizontal shear tests of the repaired laminates indicated that thorough sanding and a commonly used sheet adhesive restored the original laminate strength. As an additional aid in insuring a good repair, three 6.35 mm (0.25 inches) bolts were placed through each repaired piece between the splice region and the fiberglass end grip region. All the delaminated splice pieces were repaired using this procedure. Figure 7 is a photograph of a tension (seven bolts) and a compression (five bolts) specimen.

3.2.1 Nondestructive Testing

After each wide panel was cured and before the fiberglass end grips were bonded in place, the panels were ultrasonically inspected. The results of the inspection were not conclusive because of the large thickness of the panels and the presence of the aluminum core and fiberglass. The inspection did, however, indicate a significant difference in transmission between the two halves of the wide tension panel. This difference was caused by the mylar film that was left in the laminate.

3.3 FATIGUE SPECTRUM GENERATION

A flight-by-flight random load sequence was generated from a gust load-exceedance and a ground-air-ground (GAG) cycle specified by NASA. For a transport aircraft, gust loads and the GAG cycles are the primary source of fatigue loadings. The fatigue lifetime for such a structure was specified to consist of 30,000, 2-hour flights for a total life of 60,000 hours.

The gust load-exceedance curve provided by NASA is shown in Figure 8. The exceedance data is plotted as occurrences per 1000 flight hours versus $(P_A/P_M)^2$ where, P_A = alternating load and P_M = mean load. The maximum value of alternating load is

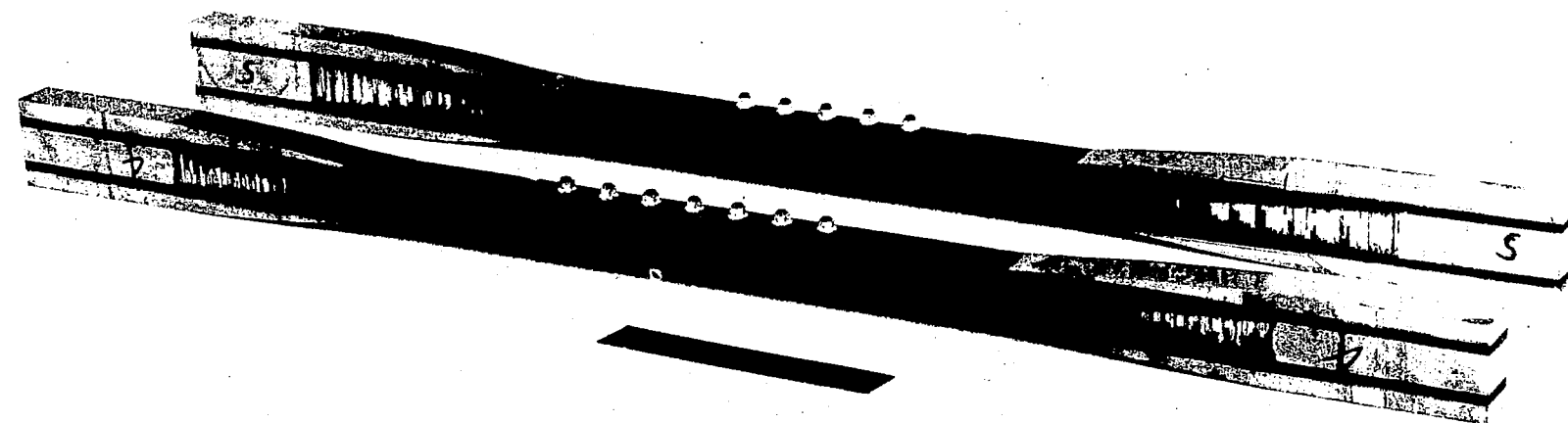


Figure 7 Tension and Compression Joint Specimens

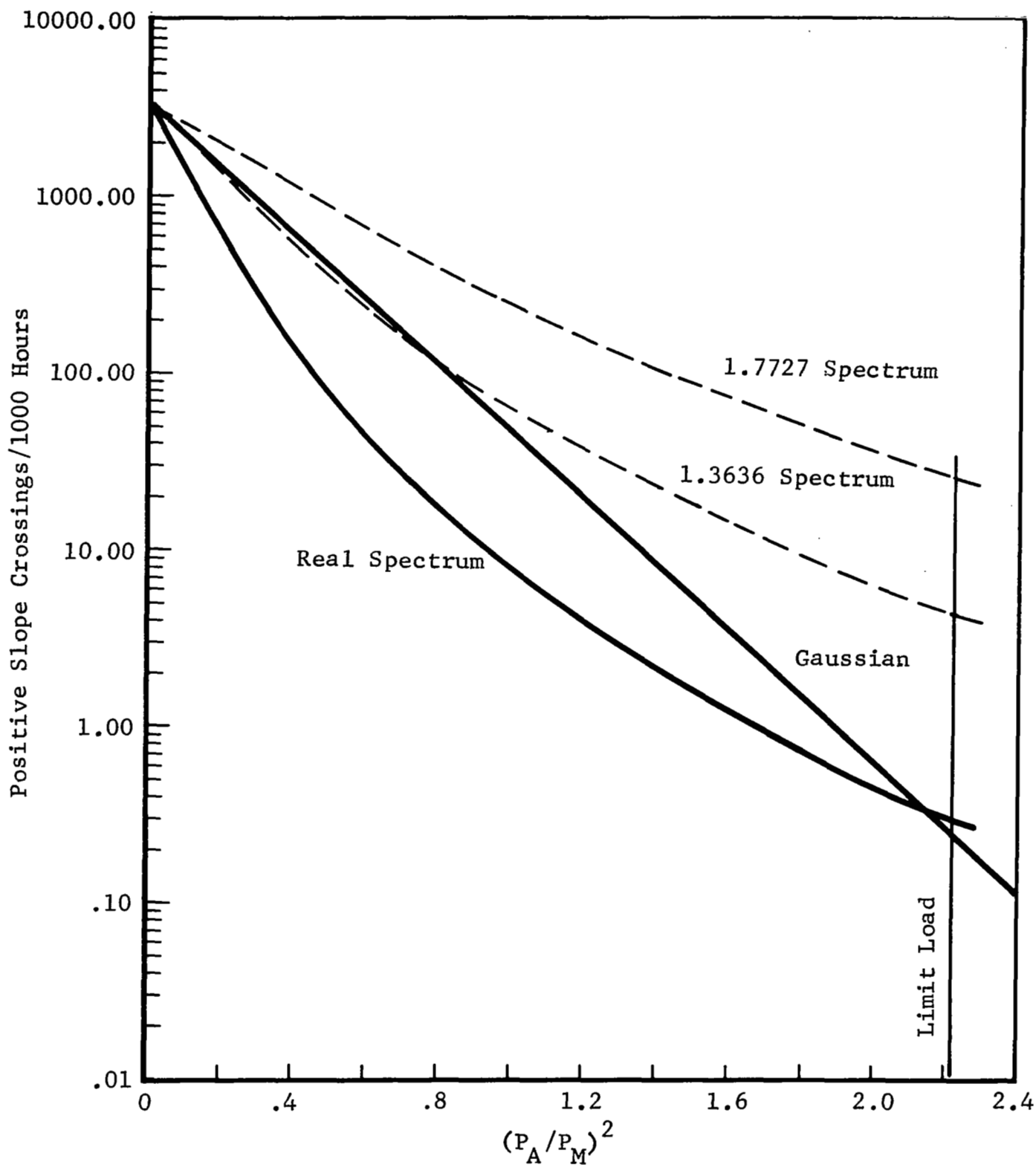


Figure 8 Transport Load Spectrum

$P_A/P_M = 1.5$. From previous experience with random load flight simulations, a spectrum of approximately 500,000 loads has been found adequate for flight simulation. The lower $(P_A/P_M)^2$ end of the exceedance curve was brought into the vertical axis at approximately 3300 positive slope crossings per 1000 hours instead of an indicated higher level. This reduces the number of low loads in the spectrum in order to arrive at approximately 500,000 loads for the fatigue lifetime history.

The straight line in Figure 8 represents a Gaussian process with the same end point. Any straight line with the same end point could have been used in the following process. The curved NASA load-exceedance curve is simulated with this Gaussian exceedance curve to arrive at the random load sequence. Then, the Gaussian loads are transformed to the real loads by means of a mapping function curve (Figure 9). The mapping function is obtained from Figure 8 by picking off corresponding points (same occurrence level) on the real and Gaussian spectra. The mapping function was assumed to be the same for both positive and negative deviations from the mean load (i.e. equal chance of gust causing + or - change from mean load).

The maximum and minimum loads for the GAG cycles were specified as P_M to $-1/2 P_M$ for the lower wing surface and $-P_M$ to $1/2 P_M$ for the upper wing surface. One GAG cycle was specified for each flight.

An average mean load (P_M) for the spectrum was determined using $P_M = \lambda \bar{P}_M$, where, λ takes into account fuel burn and \bar{P}_M was specified as 1.051 MN/m (6000 pounds/inch). For a typical advanced transport aircraft with a gross weight of 1.2366 MN (278,000 pounds), a fuel load of 0.4003 MN (90,000 pounds), and a 25 percent fuel reserve, the maximum burn for a flight is 0.3003 MN (67,500 pounds) or 0.1501 MN (33,750 pounds) at mid-flight. Thus, λ is

$$\lambda = \frac{1.2366 - 0.1501}{1.2366} = 0.88,$$

and, the average mean load is

$$P_M = 0.88 * 1.051 = 0.925 \text{ MN/m} \quad (5280 \text{ pounds/inch}).$$

Using the Gaussian exceedance line in Figure 8 and the mapping function in Figure 9, a random load history was generated using the digital computer procedure in Reference 3. Figure 10 shows the input spectrum (same for positive and negative loads)

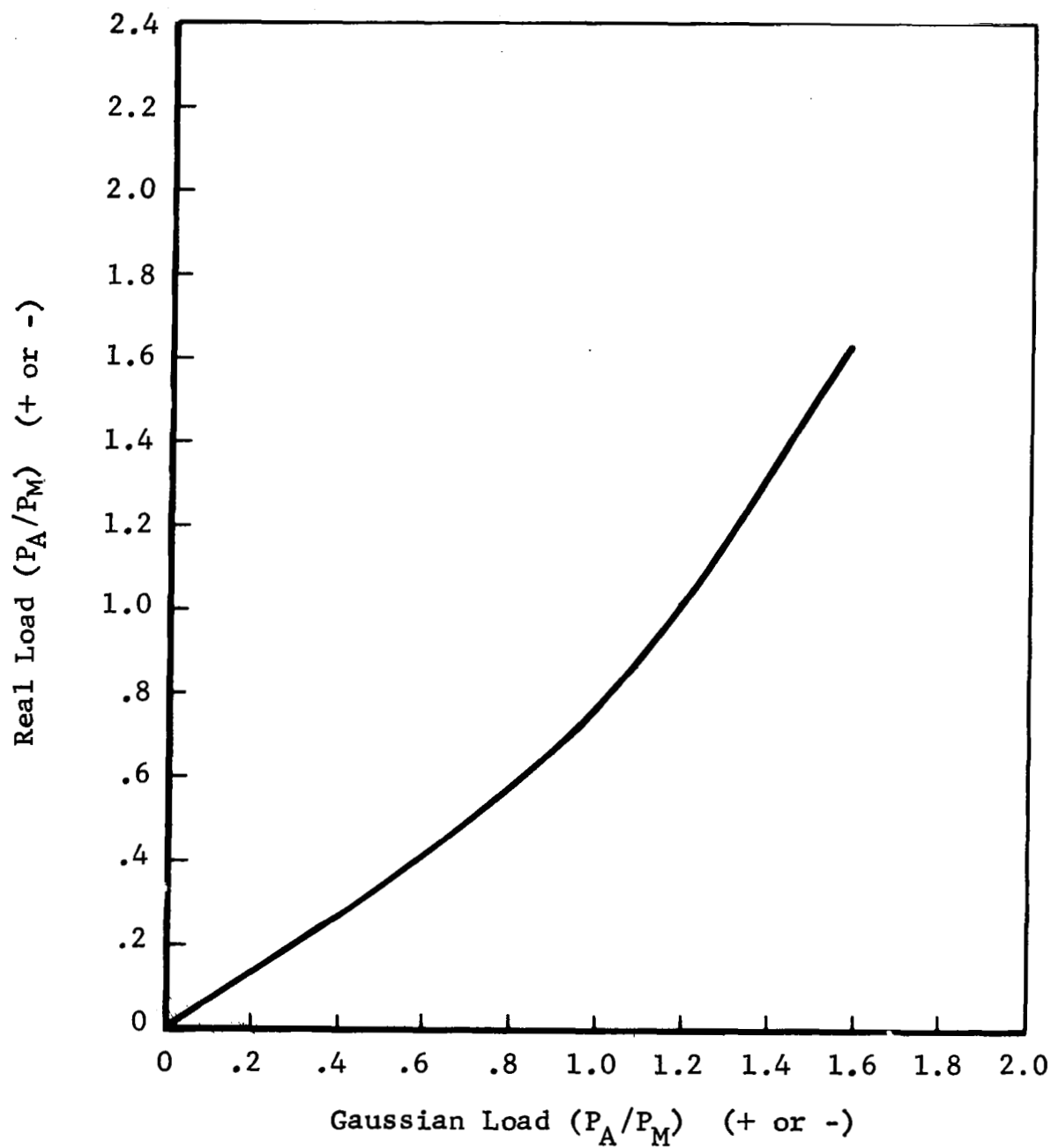


Figure 9 Mapping Function

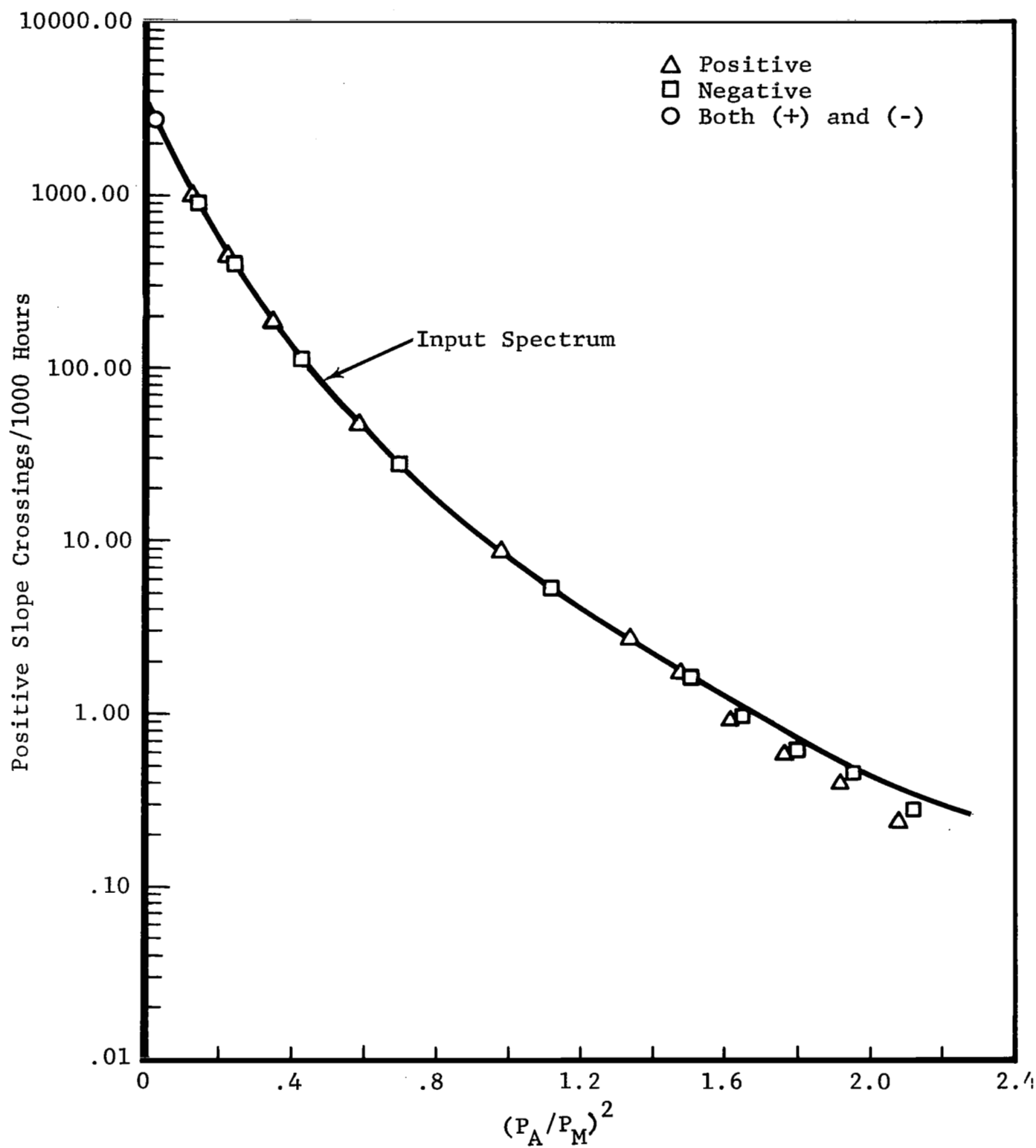


Figure 10 Comparison of Input and Output Spectra

and the spectrum calculated for the random load history. The curves show that the random load simulation accurately represents the input spectrum. The computed random load history (i.e. one lifetime or 30,000, 2 hour random load flights) contained 448,780 loads, was stored on magnetic tape and was used to conduct the fatigue tests. This tape was used for both the tension and compression tests, with a sign reversal on the loads. With a maximum test facility frequency of 5 cycles per second and 0.1 seconds for each GAG load, one lifetime on the test tape required 17.3 hours of real test time. The average frequency was 3.61 cycles per second. Figure 11 shows one of the flights from the random load history.

3.4 LABORATORY TEST EQUIPMENT

The laboratory test equipment consisted of a load control system that produces the random load signal and test fixtures (including loading rams) that hold the specimens and apply the loads. A schematic of the test equipment is shown in Figure 12.

3.4.1 Load Control System

A photograph of the load control system which was designed and built by the Fort Worth Division for fatigue testing is shown in Figure 13. This computer-controlled system utilizes a Varian 620-i general purpose digital computer, a magnetic tape reader and a teletypewriter. A unique program for the Varian computer has been developed to control the load fixtures from data supplied by the magnetic tape unit. The computer generates the load-time history signal for the servo control system. The servo control system is a typical system consisting of servo valve, servo controller, hydraulic source, hydraulic ram and load cell to provide the feedback signal.

3.4.2 Test Fixtures

Five test fixtures were fabricated for the static and fatigue tests of the splice test specimens. Figure 14 shows one of the compression test specimens installed in one of the loading fixtures. Each of the test fixtures was controlled with separate load control systems from a single computer

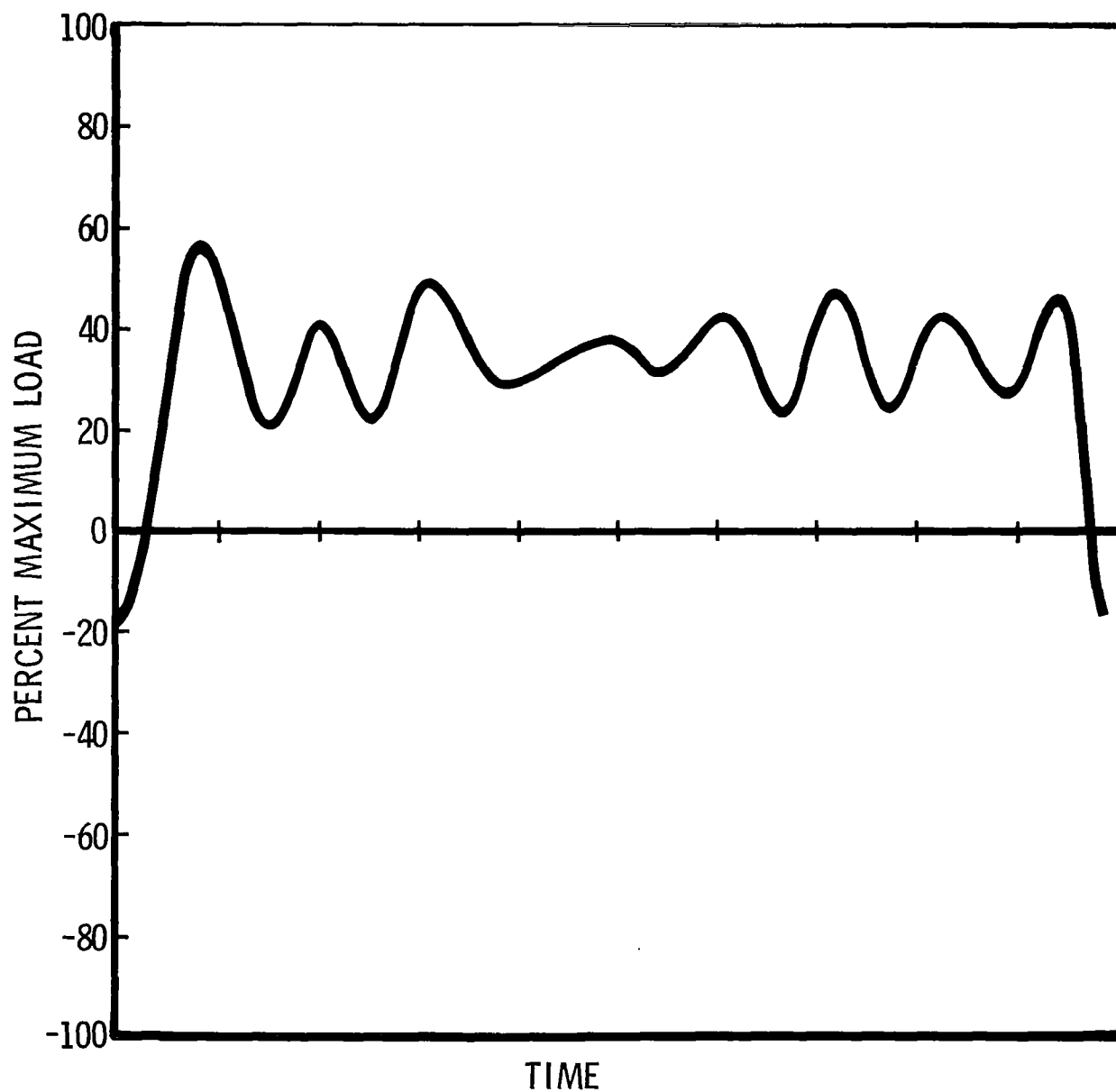


Figure 11 One Flight of Random Load History

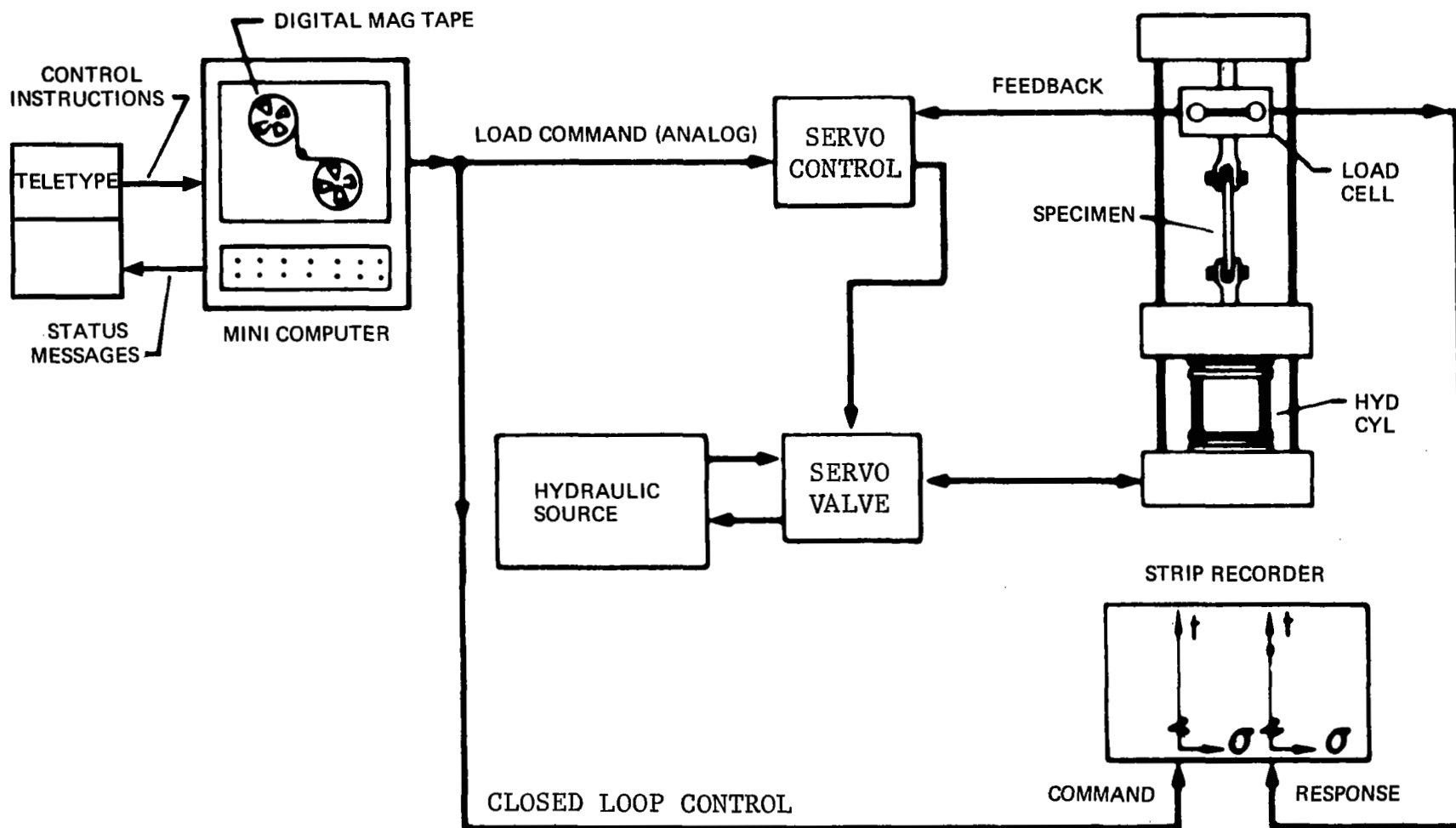


Figure 12 Schematic of Closed Loop Test Equipment

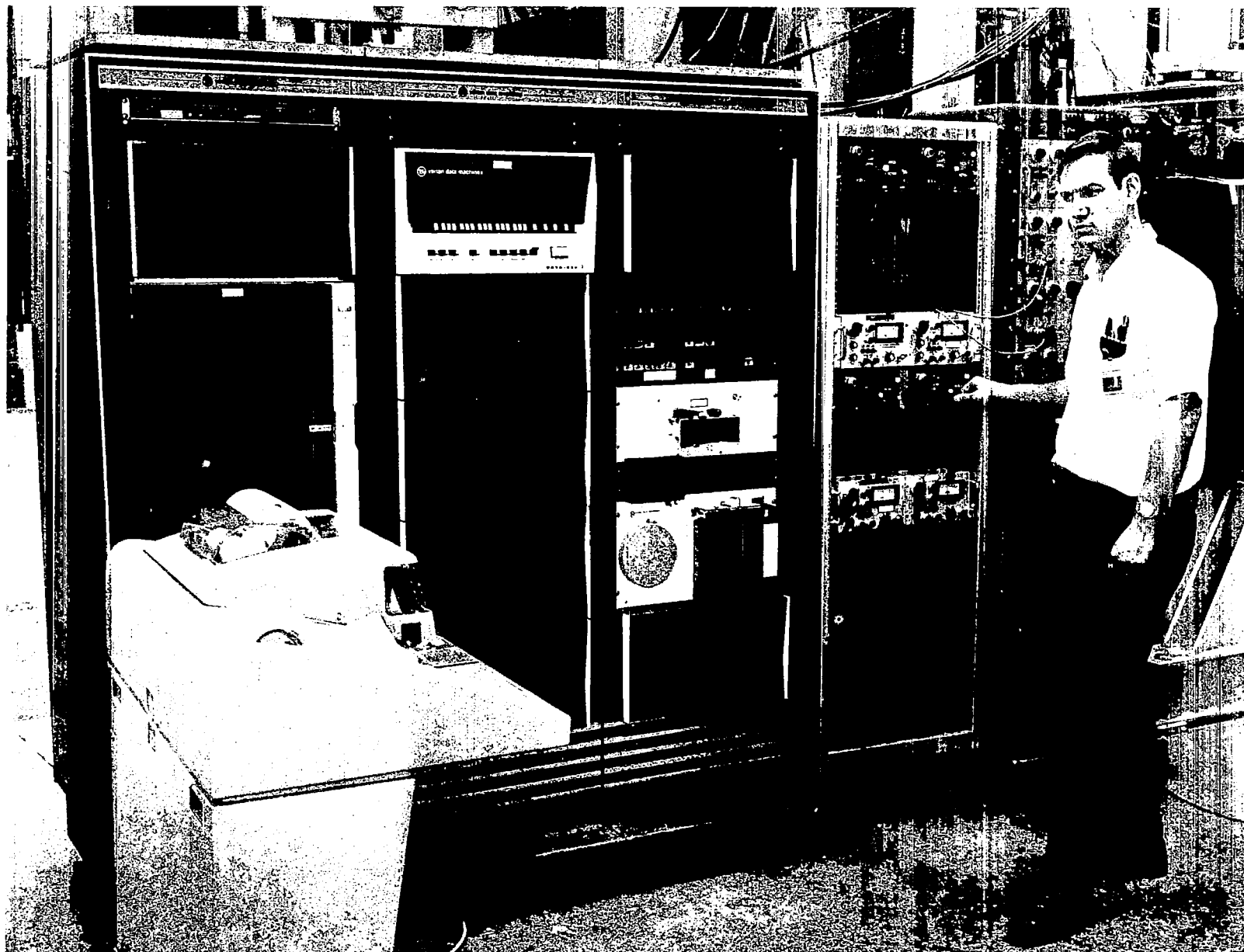


Figure 13 Load Control System

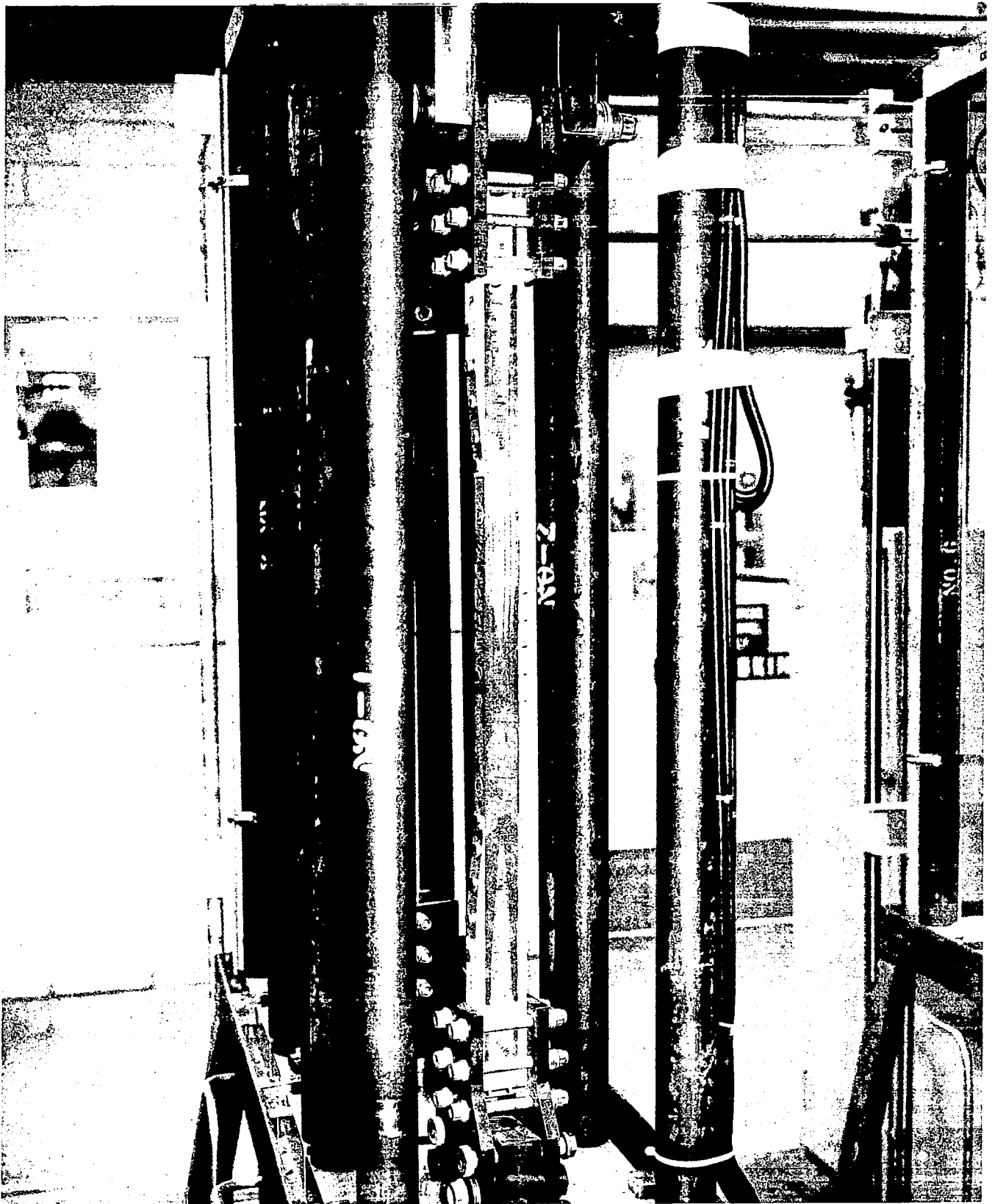


Figure 14 Test Fixture

generated signal. The loads were introduced through bolted, serrated steel plates at each end of the specimen. The specimen was attached to the load cell by a steel clevis to minimize loads caused by misalignment. This load cell provides the feedback signal to close the testing loop. Aluminum side plates were used to stabilize the compression specimens during testing. These were not required for the tension specimens even though compression loads occurred during the GAG cycles.

3.5 STATIC TEST RESULTS FOR JOINTS

Of the 20 tension and 20 compression splice specimens, 5 specimens from each set were allocated for static ultimate tests. In order to determine if the bolts were being loaded uniformly as assumed, one of the specimens was coated with a photoelastic material. Figures 15 and 16 show the fringe patterns in compression and tension on opposite faces of the test specimen. The uniformity of these patterns indicate that the bolts were being loaded uniformly and serves as a qualitative check on the design and fabrication of the specimens. Because of end grip problems and system malfunctions, two tension and two compression specimens were lost.

3.5.1 End Grip Problems

Figure 17 shows that a compression specimen that failed prematurely in the end grip region at 93.4 kN (21,000 pounds) compression. The failure initiated at the front end of the solid fiberglass block. In this first test, the grips extended beyond the fiberglass block and the core was crushed. In the second test, when the end of the grips were placed exactly at the end of the fiberglass block, the specimen failed similarly at 87.2 kN (19,600 pounds) compression. A tension specimen which was tested next failed at 85.4 kN (19,200 pounds) tension. Figure 18 shows that this failure also initiated at the front edge of the fiberglass block. At this point it became obvious that the fiberglass block was transferring a significant amount of load and causing a large stress concentration at the front edge of the block. In first attempting to alleviate the problem, a pin was put through the end grip in the core region. The end grips were then placed on the pin and a load applied before the end grips were tightened. This in effect takes a portion of the load around the problem area. The unfailed

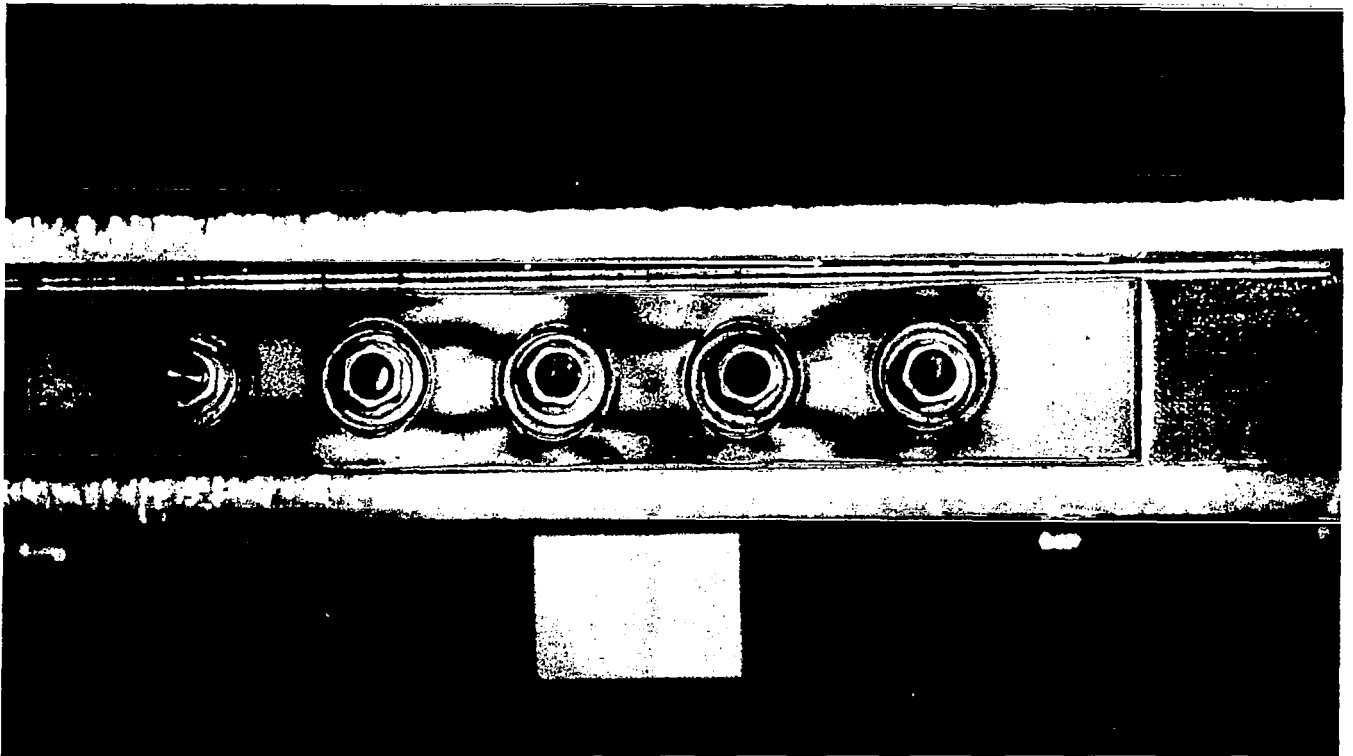


Figure 15 Compression Specimen Under Compression Load

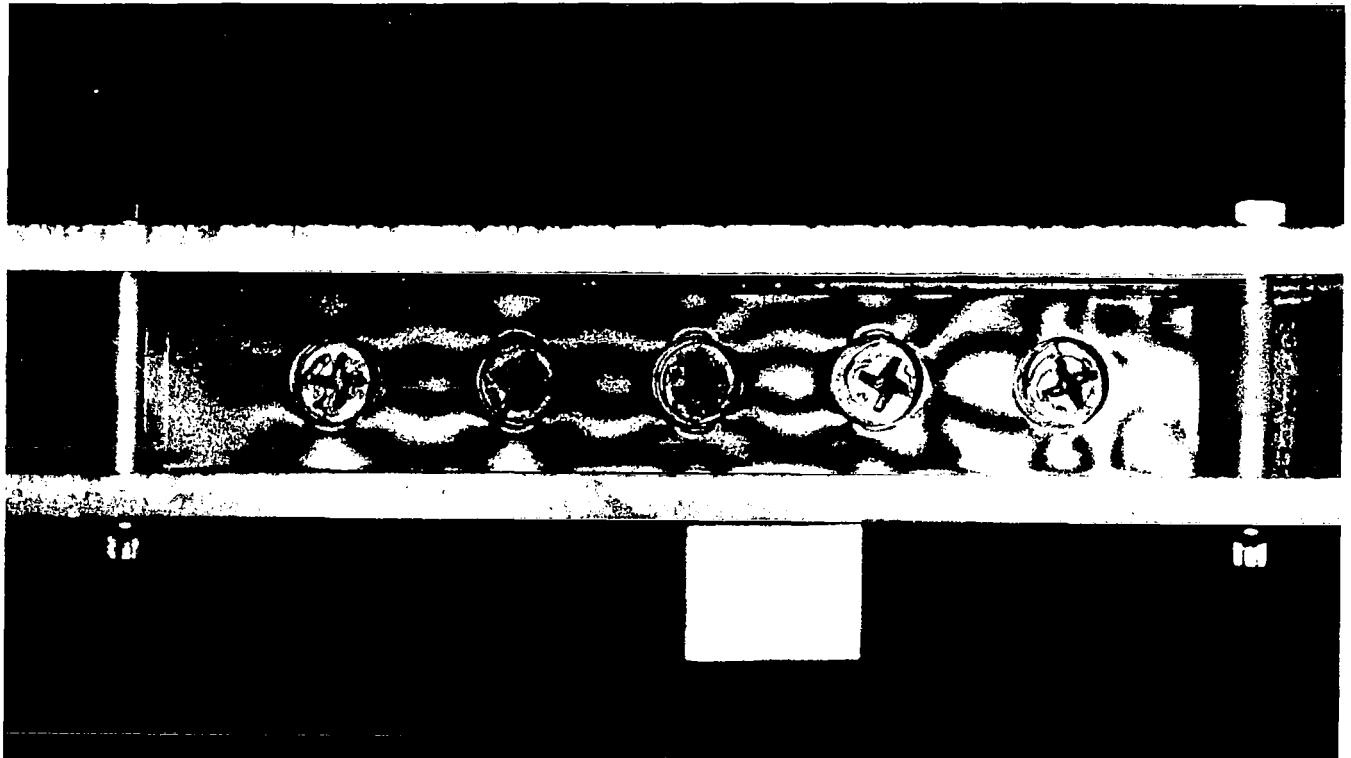


Figure 16 Compression Specimen Under Tension Load

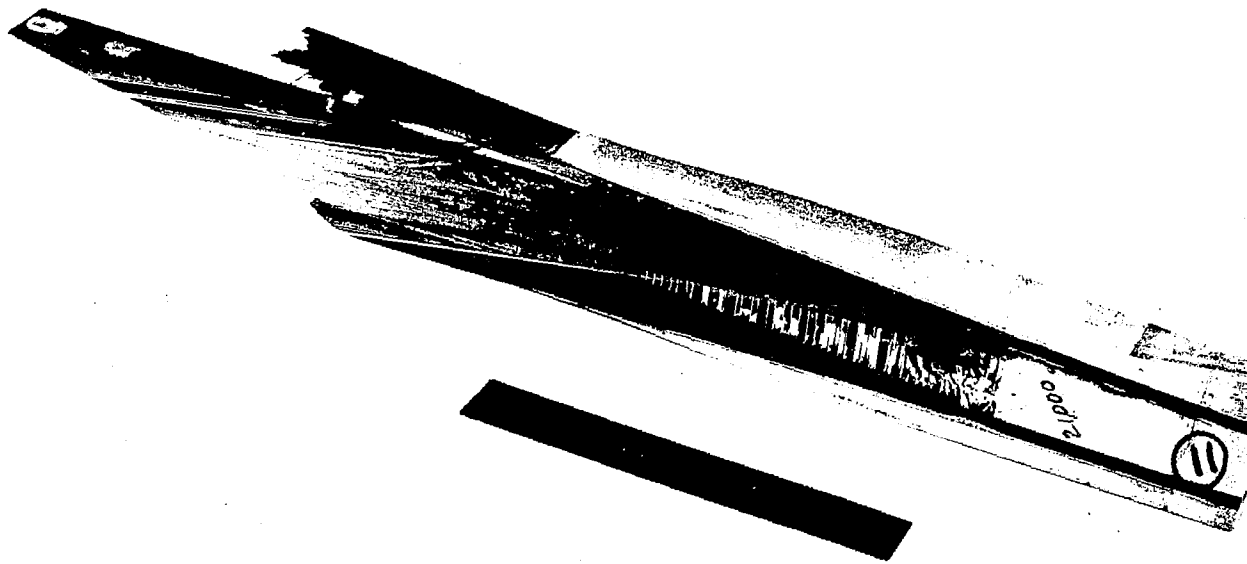


Figure 17 Static Compression Specimen End Grip Failure

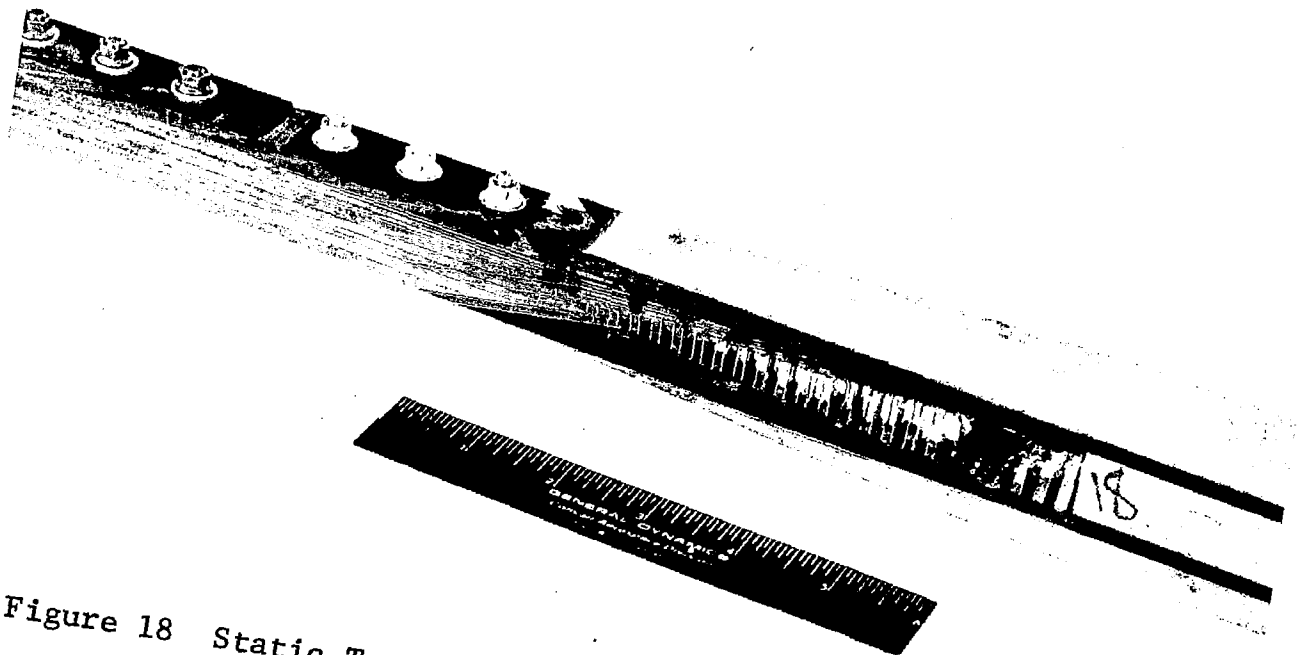


Figure 18 Static Tension Specimen End Grip Failure

pieces of two previous compression specimens were put together and loaded in the manner just described. Failure occurred in the same place at 106.8 kN (24,000 pounds) compression.

Since this fix only bypassed the problem area and did not solve the problem, an attempt was made to release the fiberglass block from the graphite skins. If this could be effected, the fiberglass would act only as a spacer for the end grips. This was the original intent of the fiberglass block. As a means of accomplishing this, saw cuts were made along the interface of the fiberglass block and the graphite skins. A thin piece of teflon with a layer of teflon impregnated glass cloth on each side was then inserted into the two saw cuts. The frictionless teflon-to-teflon surfaces reduces the load transfer and hence the stress concentration. This fix was made on the unfailed end of a compression specimen. The graphite was then cut off square just short of the scarf and tested in compression. Failure occurred at 105.9 kN (23,800 pounds) compression in a splitting mode. The remaining specimens were fixed by installing the teflon inserts. However, to further insure against end grip failures, four bolts were placed through the core area to shear the load from the graphite to the fiberglass end grips.

3.5.2 Tension

During the static tests, the relative displacement between the two pieces of the splice specimen was recorded with a clip gage. Figure 19 shows a typical curve obtained from a tension splice specimen. In general the first large discontinuity was called failure. If a specimen did not fail catastrophically at the first large discontinuity in the curve, the point of discontinuity was called failure. A typical static failure of a tension splice specimen is shown in Figure 20.

The initial static strengths of the three static tension specimens are shown in Table II, The Weibull shape (α_0) and scale (β_0) parameters for these three tests are 60 and 102.8 kN (23,100 pounds), respectively. A mean strength of 101.9 kN (22,900 pounds) for the three tests compares favorably with the design ultimate load of 100.1 kN (22,500 pounds). The high α_0 indicates very low scatter although three tests are not sufficient to accurately estimate the shape parameter.

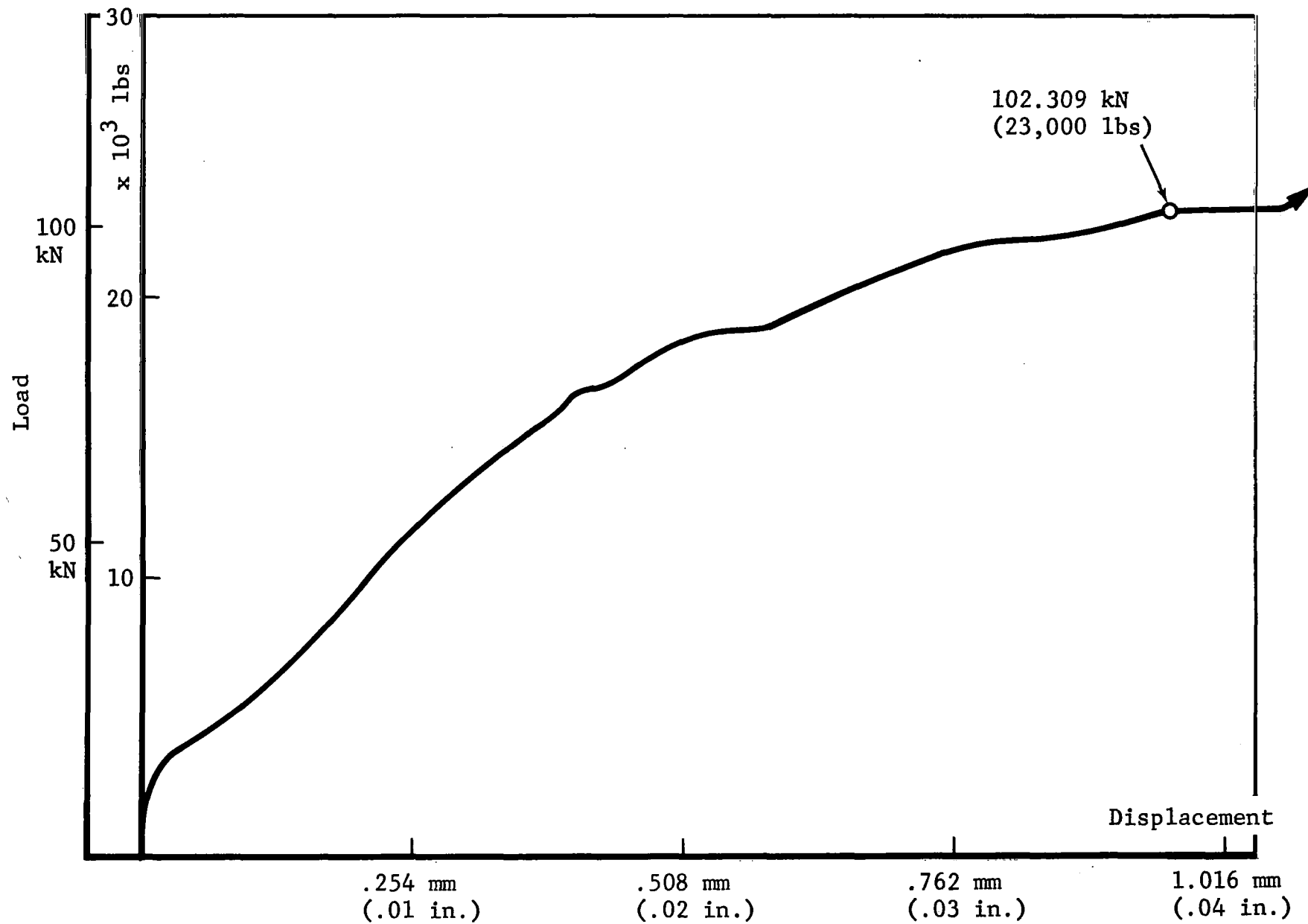


Figure 19 Typical Load-Displacement Curve for Tension Splice Specimen

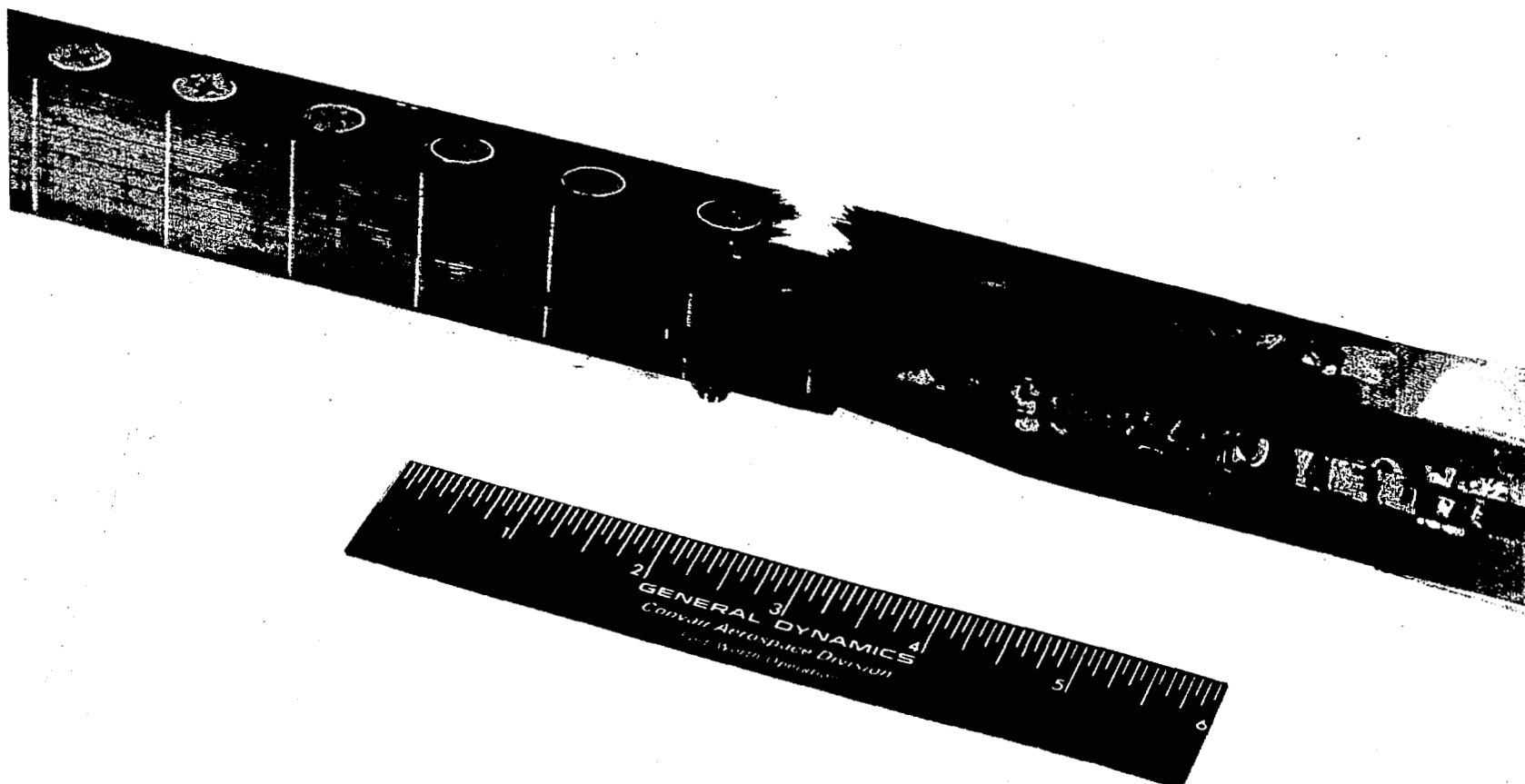


Figure 20 Static Tension Failure

Table II STATIC TEST RESULTS
FOR JOINT SPECIMENS

Tension Static
Strength, kN (lbs.)

100.1 (22,500)
102.3 (23,000)
103.2 (23,200)

$$\alpha_o = 60$$

$$\beta_o = 102.8 \text{ kN (23,100 pounds)}$$

α_o = Weibull Shape Parameter

β_o = Weibull Scale Parameter

Compression Static
Strength, kN (lbs.)

99.6 (22,400)
100.5 (22,600)
101.4 (22,800)

$$\alpha_o = 109$$

$$\beta_o = 101.0 \text{ kN (22,700 pounds)}$$

3.5.3 Compression

The relative displacement between the two pieces of the joint was also monitored during the compression tests. Figure 21 shows a typical load versus displacement curve. The first successful compression specimen test was taken to a loading of 134.3 kN (30,200 pounds) or 1.34 times design ultimate. The load cell being used in the test fixture was only calibrated to 133.4 kN (30,000 pounds) so loading was halted at this point. Since this load level was near the shear capacity of the bolts, it was anticipated that the ultimate failure of the joint would be complete shearing of all bolts. An inspection of the load deflection plot (Figure 21) indicated a significant slope change at 100.5 kN (22,600 pounds). The specimen was removed from the test fixture and the holes inspected. Figure 22 shows splitting cracks in front of and behind the end bolt in the load direction. Since splitting was the critical failure mode, failure was defined as the load at the change in slope.

The static compression strengths (based on significant slope change in the load displacement curves) are shown in Table II. The Weibull shape and scale parameters are 109 and 101.0 kN (22,700 pounds), respectively. A mean compression strength of 100.1 kN (22,500 pounds). The high shape parameter again indicates very low scatter in the data.

3.6 FATIGUE TEST RESULTS FOR JOINTS

One of the purposes of the development test program was to determine the relationship between stress and life for the joint. Thus, in the first series of tests, the magnitudes of the loads in the real spectrum were multiplied by a factor of 1.3636 to cause short fatigue lives. However, fatigue failures did not occur, and the specimens were statically tested after four lifetimes. The magnitude of the loads in the real spectrum were then multiplied by a factor of 1.7727 for the next series of tests, and fatigue failures occurred in less than 1.1 lifetimes. The residual strengths and fatigue lives from these two series of tests were used to estimate parameters for the "wearout model" which was then used to predict fatigue lives for the real spectrum. Tests were run with the real spectrum to 10 lifetimes, which was much less than the 433 lifetime prediction, to determine the effect of the real fatigue spectrum on residual strength.

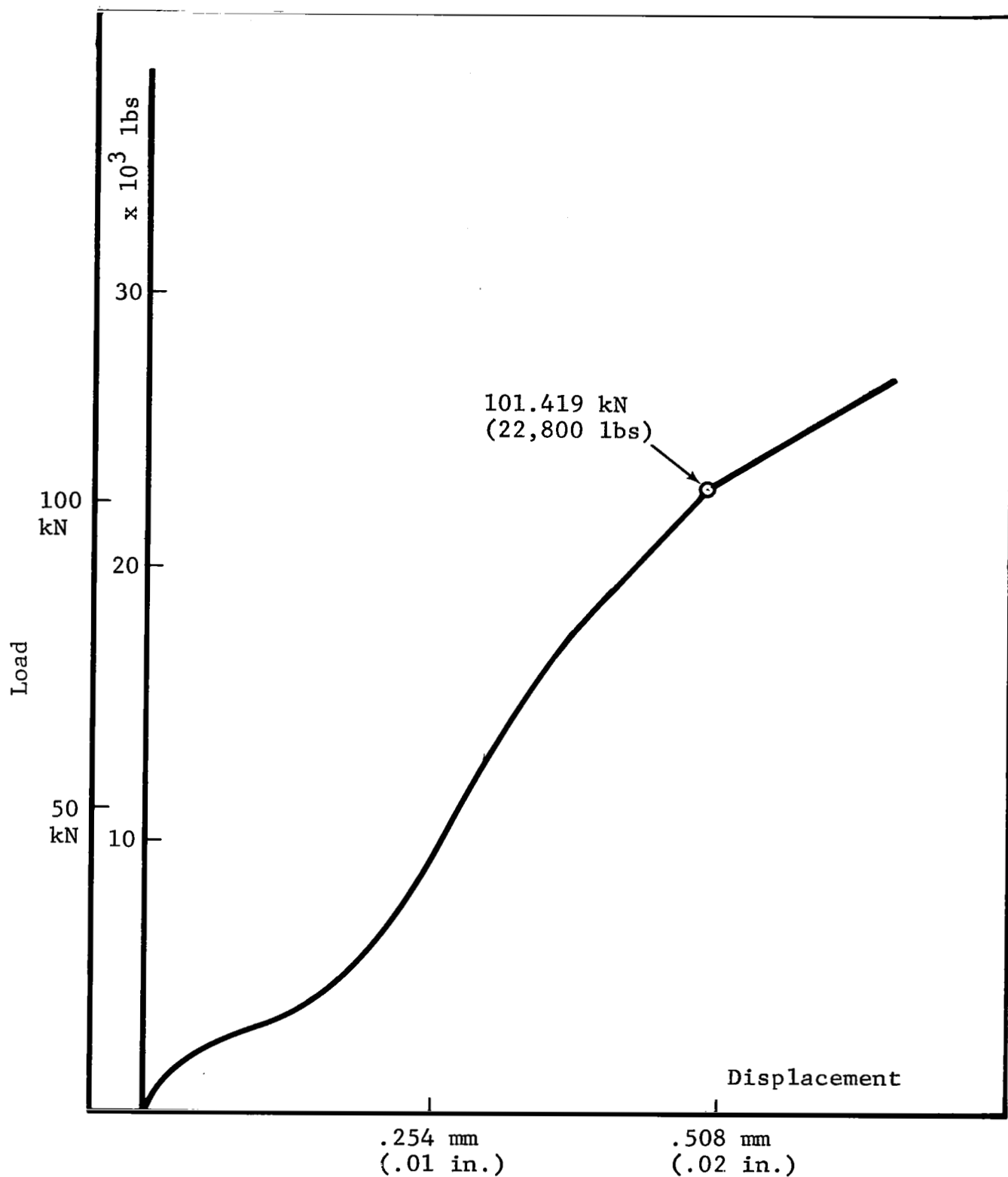


Figure 21 Typical Load-Displacement Curve for Compression Splice Specimen

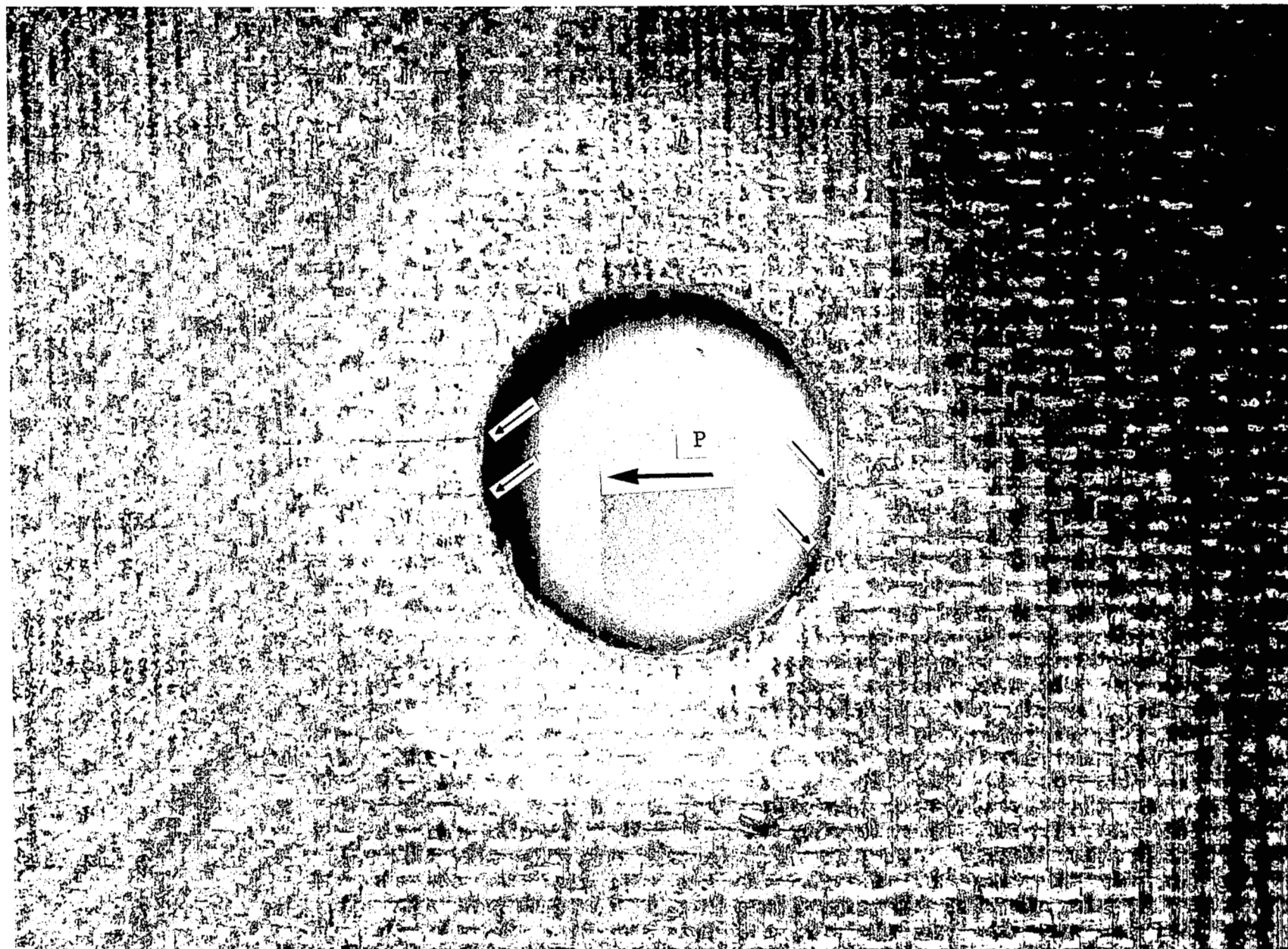


Figure 22 Splitting Failure Mode in Static Compression Specimen

In order to further test the "wearout model," tests were run for up to eight lifetimes with a magnified spectrum that was predicted to cause fatigue failures in eight lifetimes.

3.6.1 Magnified Spectra

The magnification of the loading spectrum was performed in the test laboratory and results in a scale-up of all loads in the spectrum (see Figure 8). Thus, this magnification produces larger load reversals for the GAG load cycles.

3.6.1.1 Magnification Factor of 1.3636

Five tension and five compression specimens were fatigue tested with a magnified spectrum in which the magnitude of all the loads in the real spectrum were multiplied by a factor of 1.3636. This factor raises the maximum load (limit load) in the real spectrum to 80 percent of the design ultimate load or 80.1 kN (18,000 pounds). The maximum load was reached approximately six times per aircraft lifetime. Three tension specimens and four compression specimens were fatigue tested to four lifetimes without a fatigue failure. These specimens were then statically tested to measure residual strength. Two tension specimens and one compression specimen were lost during the fatigue tests due to system malfunctions. Also, the heads of many of the countersunk NAS 1154 titanium bolts failed in fatigue during the tests. The failures occurred at the intersection of the head and shank where the net area was significantly reduced by the deep recess in the head. A change from titanium to steel bolts helped but did not eliminate the problem. The problem was finally solved by switching to NAS 584 "Hi-Torque" steel bolts which had a shallow recess that did not extend into the shank of the bolt.

The residual strength results are given in Table III. The data shows that four lifetimes of the 1.3636 magnified spectrum had a very small effect on the mean static strength of the joint specimens. The residual strength tests were again monitored with a clip gage measuring relative displacement between the splice parts. The resulting load-displacement curves were very similar to those obtained in the initial static strength tests and failure was assigned to the initial large discontinuity in the curves. Likewise, the complete failure of the tension residual strength specimens were very similar to the initial static tension specimens (see Figure 20).

Table III FATIGUE TEST RESULTS FOR JOINT SPECIMENS

TENSION		COMPRESSION	
Residual Strength at 4.0 Lifetimes, kN (lbs.) Magnification Factor = 1.3636	Fatigue Failure (Lifetimes) Magnification Factor = 1.7727	Residual Strength at 4.0 Lifetimes, kN (lbs.) Magnification Factor = 1.3636	Fatigue Failure (Lifetimes) Magnification Factor = 1.7727
96.1 (21,600)	0.465	94.3 (21,200)	0.254
99.2 (22,300)	0.625	97.0 (21,800)	0.460
105.9 (23,800)	0.670	97.9 (22,000)	0.530
	0.854	101.0 (22,700)	0.603
	1.107		0.633
	$\alpha_f = 3.10$		$\alpha_f = 2.67$
	$\beta_f = 0.835$		$\beta_f = 0.568$
α_f = Weibull Shape Parameter			
β_f = Weibull Scale Parameter			

3.6.1.2 Magnification Factor of 1.7727

Five tension and five compression specimens were fatigue tested with a magnified spectrum in which the magnitude of all the loads in the real spectrum were multiplied by a factor of 1.7727 (1.3×1.3636). The spectrum was truncated at a maximum load of 80 percent of ultimate or 80.1 kN (18,000 pounds), i.e. all loads that would have exceeded the maximum load were reduced to the maximum load. In the resulting spectrum, the maximum load was reached approximately 150 times per lifetime. Figure 23 shows a load-time trace of the 1.3636 and 1.7727 magnified spectra. The increase in severity with magnification factor is apparent.

The five tension specimens were tested first. Two specimens failed catastrophically at 0.465 and 0.670 lifetimes. One of these failed specimens is shown in Figure 24. The tests of the three remaining specimens were continued until 0.854 lifetimes when the test monitor heard a bolt snap in one of the specimens. This particular test was stopped and the specimen inspected. Two bolts were found to be broken and all the bolt holes in the specimen were damaged. The two broken-bolt holes were elongated by approximately 10 percent. Thus, the bolts probably broke in bending fatigue due to the excessive clearances. Figure 25 shows an X-ray radiograph of the two broken-bolt holes in each part of the splice, viewed from the inner surfaces. The extent of the fatigue damage is indicated by the dark areas around the holes. The dark areas were made by applying an opaque liquid die (tetrabromoethane) to the damaged area around the bolt holes prior to X-raying the specimen. The liquid die propagated into the cracks and delaminations by capillary action, causing the damaged areas to show up as dark zones. This NDE method is described in more detail in Reference 4. The specimen was considered to be failed and the test terminated at this point because of the large amount of damage. Based on these observations, fatigue failure of the remaining specimens (tension and compression) was set at first bolt failure. Testing of the last two tension specimens was continued and the fatigue lifetimes for first bolt failure are given in Table III. The broken bolts were replaced in these last two specimens and testing was continued. The joints eventually failed in net tension at an average lifetime of approximately 40 percent longer than the time to first bolt failure. Figure 26 shows one of these last two specimens after final failure. It should be noted that the 40 percent difference in life between first bolt and final failure was obtained with the highly magnified spectrum (1.7727).

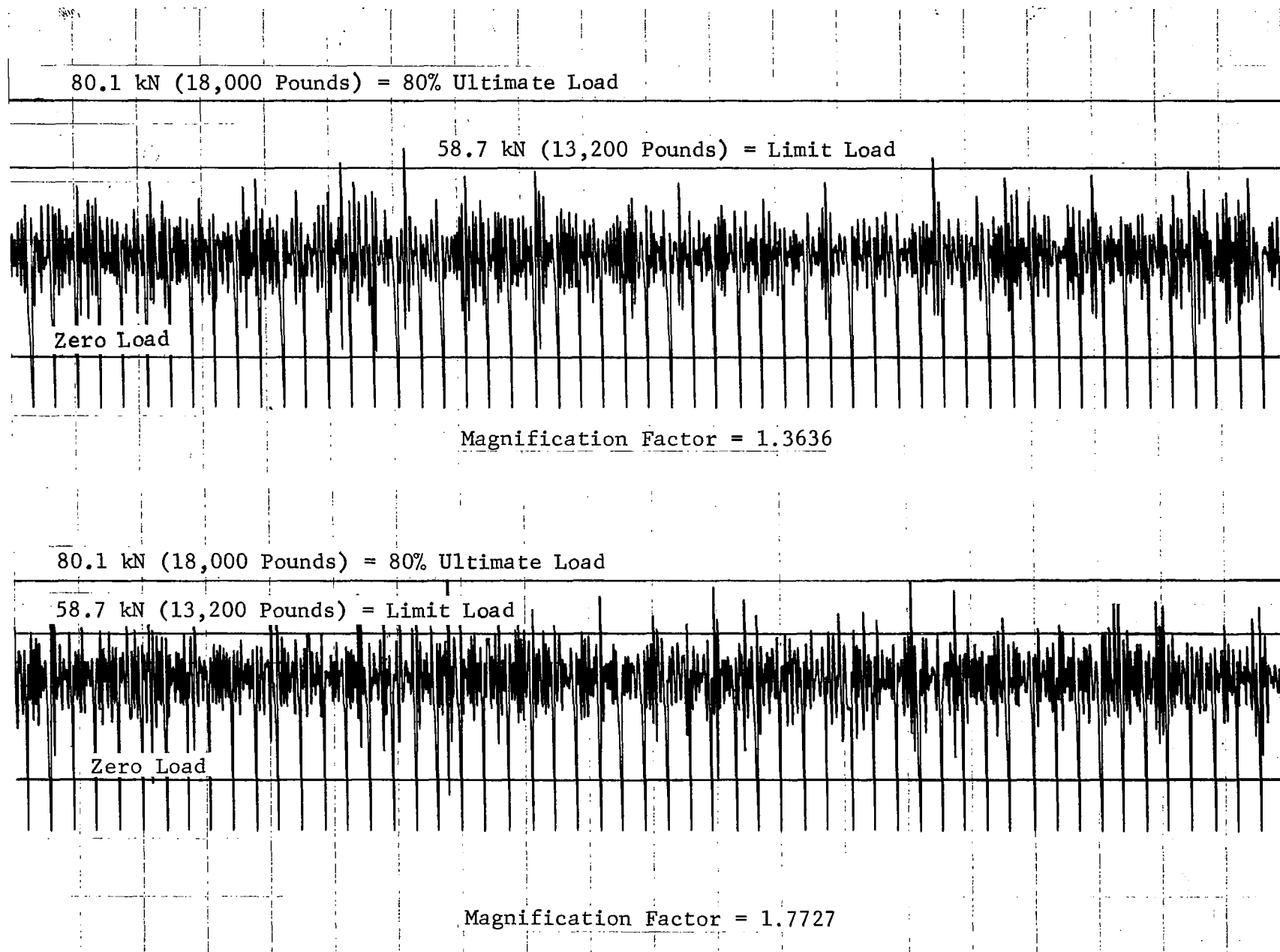


Figure 23 Spectrum Magnification Effects

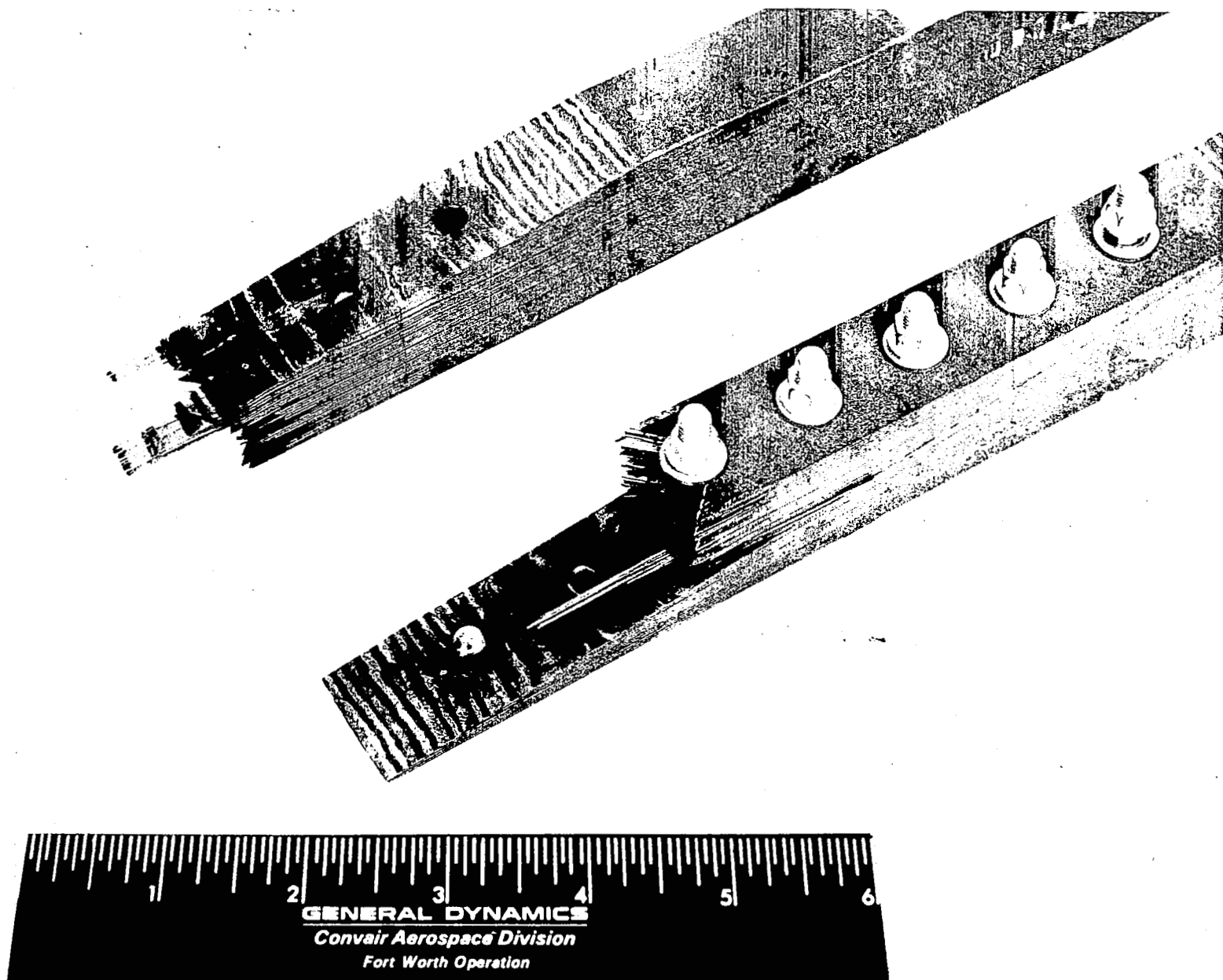


Figure 24 Tension Fatigue Failure at 0.465 Lifetimes

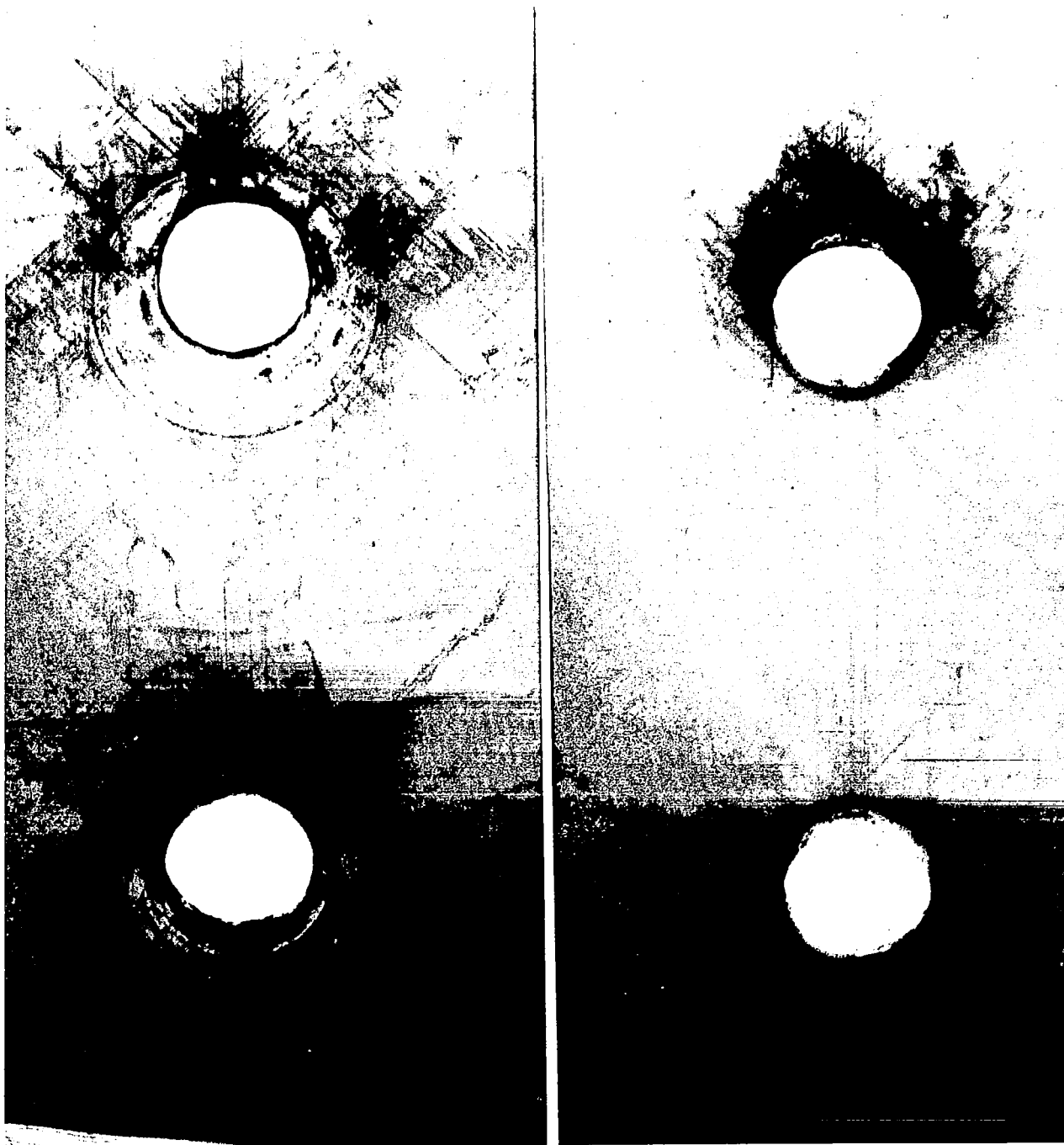


Figure 25 Tension Fatigue Damage at 0.854 Lifetimes

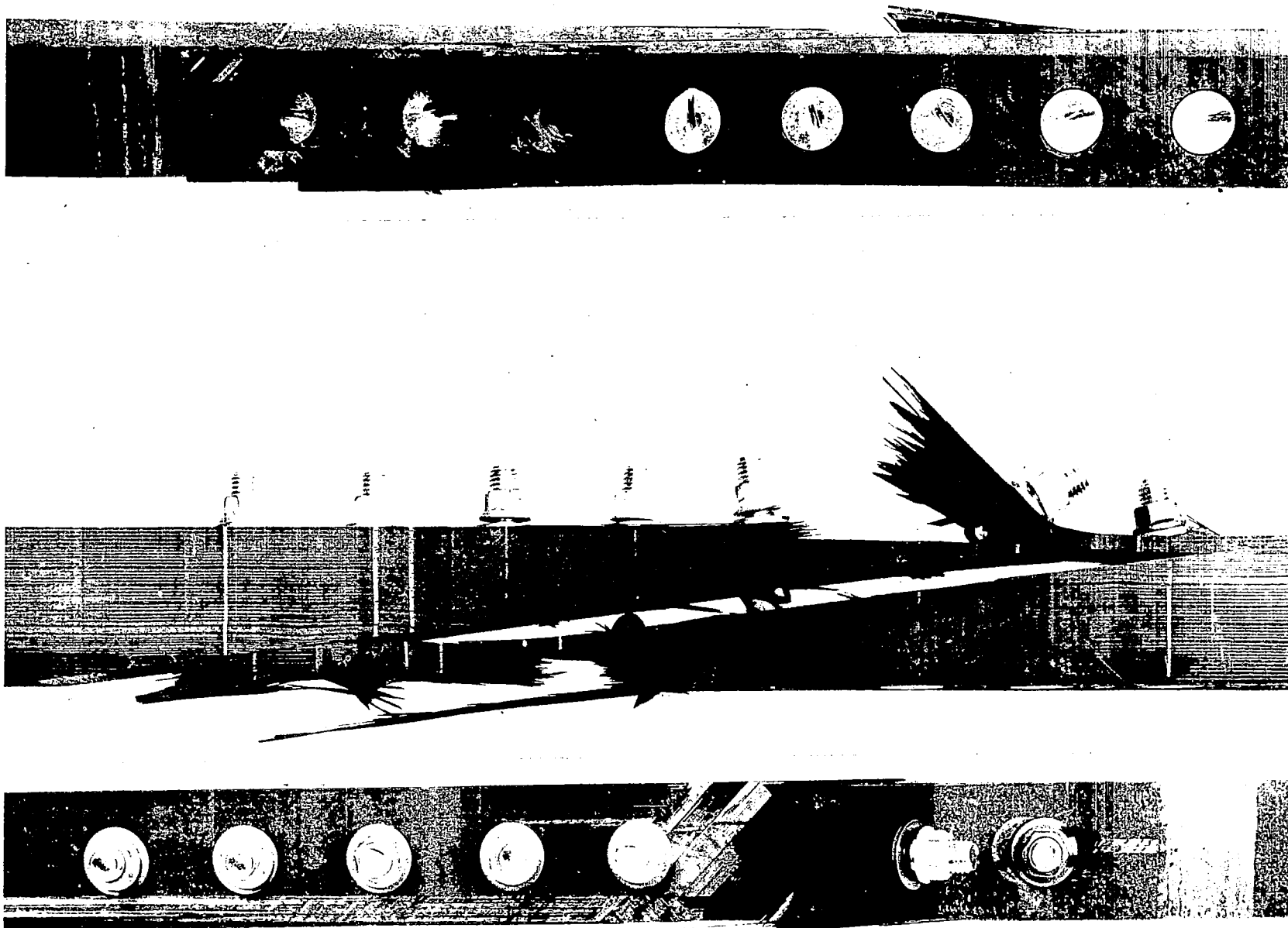


Figure 26 Tension Fatigue Failure at 0.862 Lifetimes

Next, five compression specimens were tested. After first bolt failure, several of the specimens were inspected for damage around the holes. These inspections indicated that the same failure mechanism was present in both the tension and compression specimens. Thus, the compression lifetimes reported in Table III are for first bolt failure. The results show that the life to first bolt failure of the tension specimens is about 50 percent greater than that of the compression specimens.

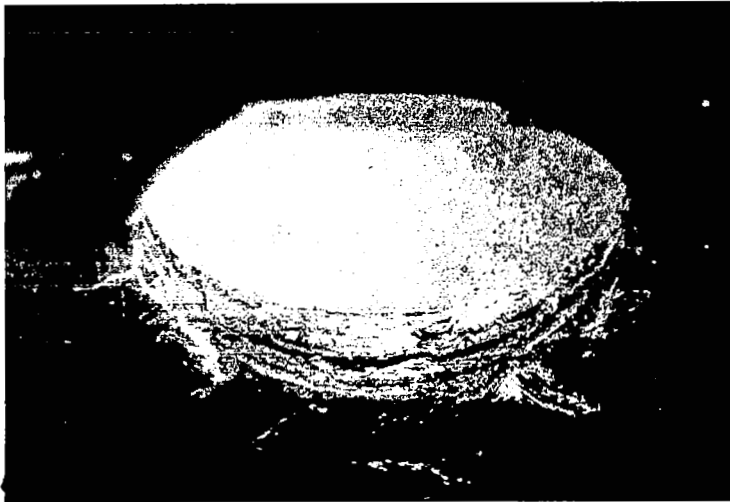
3.6.1.3 Magnification for Eight Lifetimes

Two tension and one compression specimen were fatigue tested with magnified spectra in which the magnitude of all the loads in the real spectrum were multiplied by factors of 1.4258 for tension and 1.3765 for compression. The magnification factors were calculated for a mean life of eight lifetimes using the wearout model discussed in Section 3.6.3. The spectra were truncated at a maximum load of 80 percent of design ultimate.

The compression fatigue test was stopped at 8 lifetimes. Bolt failures indicative of bearing damage occurred at 4.024, 6.437, 6.599 and 7.351 lifetimes. At the first bolt failure (4.024 lifetimes) the specimen was taken apart and inspected for damage. Some bearing damage was visible and the holes had been elongated about 3 to 4 percent. However, based on the first break as failure criteria, the life of the specimen was 4.024 lifetimes or about 50 percent of the expected mean life. Each of the broken bolts was replaced and the test continued to 8 lifetimes. The specimens was inspected again and the bolt holes had elongated 5 to 6 percent. The specimen was static tested to failure in compression. A nonlinear point occurred in the load-deflection curve at 102.3 kN (23,000 pounds). The specimen failed in the end grip region at 117.0 kN (26,300 pounds). One of the tension specimens was lost at 3.844 lifetimes when the feedback signal from the load cell was accidentally interrupted. A maximum load of 108.4 kN (24,380 pounds) was recorded at failure. Two bolt heads had failed earlier at 3.177 and 3.580 lifetimes; however, the holes were inspected at 3.580 lifetimes and no appreciable bearing damage was found. The test of the other tension specimen was stopped at 4.010 lifetimes when one of the bolts broke due to bearing damage in the hole. The specimen was also cracked longitudinally. Figure 27 shows the crack in the specimen and the damage around the holes at the thin end of each splice piece. The broken bolt was replaced and the test continued. Final failure of the specimen occurred at 6.049 lifetimes.



Side View Showing Longitudinal Crack



Thin End Countersunk Hole - View From Inside Scarf



Thin End Hole - View From Inside Scarf

Figure 27 Tension Splice Damage at 4.010 Lifetimes

3.6.2 Real Spectrum

One tension and one compression specimen were fatigue tested to 10 lifetimes with the real spectrum loading and then were statically tested to measure residual strength. The bolts in the tension specimen (checked periodically) lost no torque and no bolt problems of any type occurred through the 10 lifetimes of fatigue testing. Also, no bearing damage was found in the bolt holes upon inspection after the test concluded. During the static residual strength test, nonlinearities occurred in the load-deflection curve at 74.7 kN (16,800 pounds) and at 90.7 kN (20,400 pounds) before final failure at 100.1 kN (22,500 pounds). During the compression real spectrum test, several bolt heads or nuts cracked off; however, no bolts failed in the shank and no bearing damage was found around the holes upon inspection at the end of the test. During the static residual strength test a nonlinear point occurred in the load-deflection curve at 102.8 kN (23,100 pounds) before final failure at 128.6 kN (28,900 pounds) in the end grip region of the specimen.

3.6.3 Wearout Model

The wearout model of References 5 and 6 was used to analyze the magnified spectra fatigue and residual strength data in Tables II and III and to predict the life under the real spectrum. This model relates the residual strength and fatigue lifetime distributions through a kinetic fracture hypothesis based on the assumptions that all materials in a structure contain pre-existing flaws and that failure is caused by a reduction in strength due to the growth of these flaws. These flaws were assumed to grow in a deterministic manner depending upon the material state and its environmental history. A discussion of the input parameters for this model follows.

Estimates of the shape parameter α_0 and scale parameter β_0 for the Weibull distribution are given in Table II for the tension and compression initial static strength data. The shape parameters α_0 are probably larger than that commonly reported for fiber controlled laminates (i.e. α_0 approximately 30) because of the small number of test points. Thus, an α_0 of 30 was used in the wearout model as a conservative estimate for both tension and compression data sets. The shape α_f and scale β_f parameters for the fatigue lifetimes under the magnified

spectra are given in Table III. Because the scale parameters α_f were nearly equal and because the same failure mechanism was active in both the tension and compression specimens, a data pooling technique was used to determine an α_f for the combined tension and compression data. In this technique, each of the five tension and compression lifetime data points was divided by β_f for the tension and compression lifetimes, respectively. The resulting 10 data points were then used with a least-squares technique to estimate an α_f of 3.36. The crack growth rate exponent r in the wearout model is given by

$$r = \frac{\alpha_o}{2 \alpha_f} + 1$$

$$r = \frac{30}{(2)(3.36)} + 1$$

$$r = 5.46.$$

With this basic input data (α_o , β_o and r), the wearout model was used to produce residual strength (load) versus fatigue lifetime plots. Figures 28 and 29 show these plots for the tension and compression specimen data, respectively. The residual strength curves (i.e. probability of survival curves) were calculated using the wearout model for both the 1.3636 and 1.7727 magnified spectra.

The wearout model can also be used to predict the effects of load level changes through use of the load magnification parameter A_1 :

$$\beta_{f_{\text{real}}} = \beta_{f_{A_1}} (A_1)^{2r}$$

where $\beta_{f_{\text{real}}}$ is the scale parameter for the real spectrum with a load magnification parameter A_1 of 1.0. For the tension data set $A_1 = 1.7727$, $\beta_{f_{A_1}} = 0.835$ and $r = 5.46$, thus

$$\beta_{f_{\text{real}}} = 0.835 (1.7727)^{10.92}$$

$$\beta_{f_{\text{real}}} = 433 \text{ lifetimes.}$$

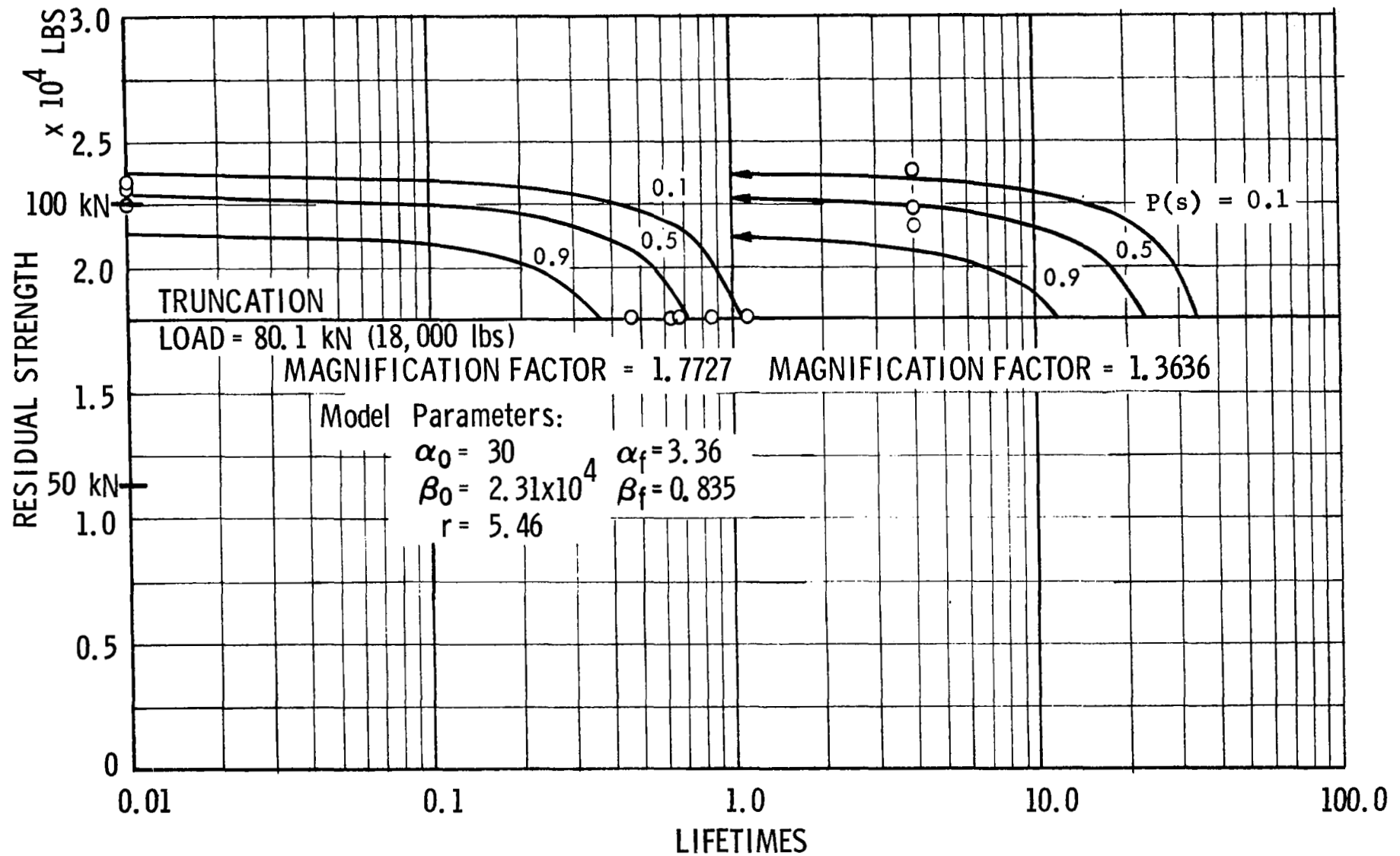


Figure 28 Wing Splice Tension Joint Data

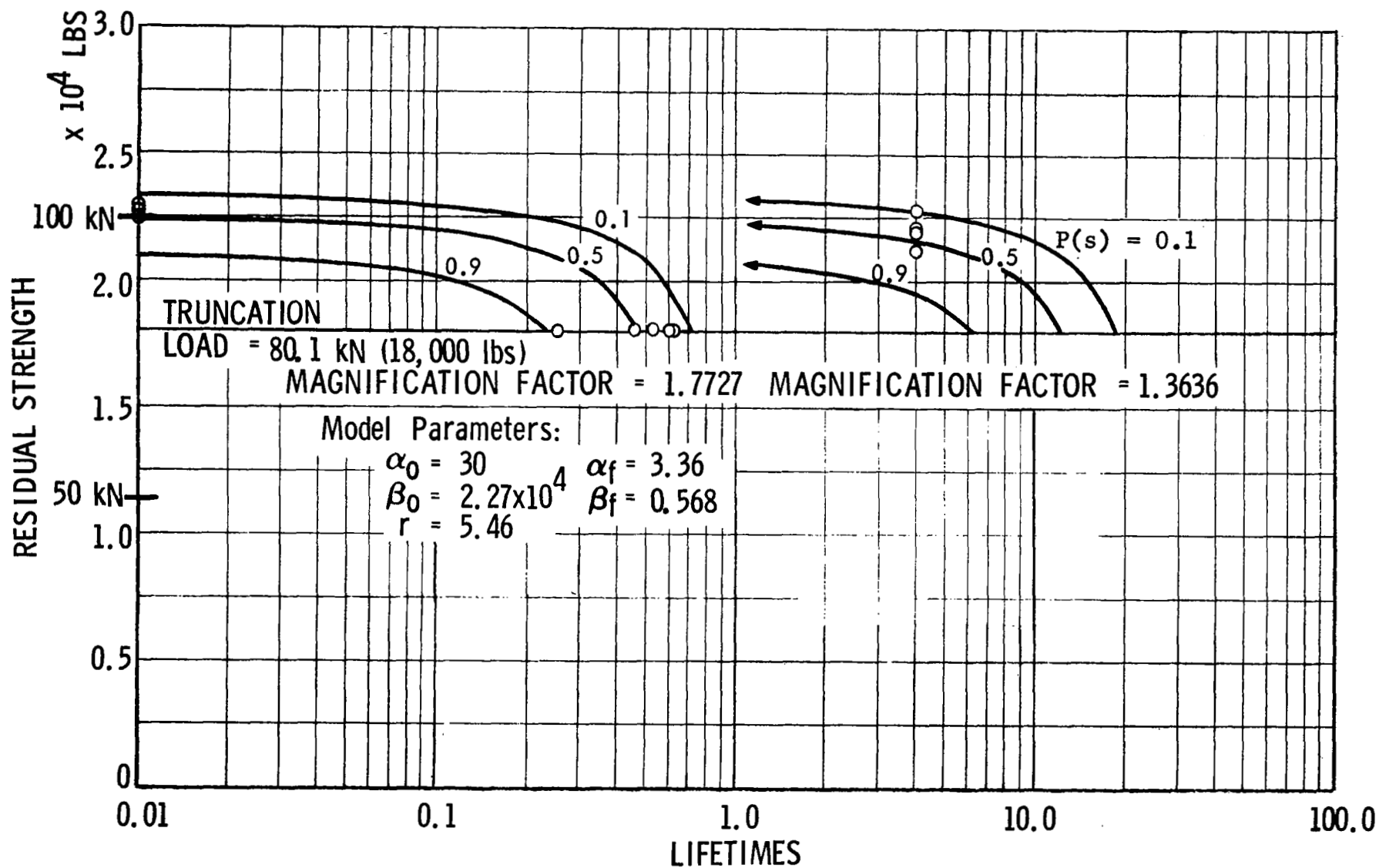


Figure 29 Wing Splice Compression Joint Data

Therefore, under the real tension fatigue spectrum with no load magnification (i.e. maximum load in spectrum equal to limit load), the wearout model predicts a fatigue life scale parameter of 433 lifetimes. Similarly, for the compression data set, the wearout model predicts a fatigue life scale parameter of 295 lifetimes under the real compression fatigue spectrum. Thus, the long life characteristics of composite laminates have been transferred to the splice concept.

The wearout model was also used to predict magnification factors that would give a mean life of 8 lifetimes for the tension and compression splice specimens. The mean (\bar{x}) for the Weibull distribution is given by

$$\bar{x} = \beta_f \Gamma\left(\frac{1}{\alpha_f} + 1\right)$$

where, Γ is the gamma function and $\left(\frac{1}{\alpha_f} + 1\right)$ is its argument. For $\alpha_f = 3.36$ and $\bar{x} = 8$,

$$\beta_f = 8 / \Gamma\left(\frac{1}{3.36} + 1\right)$$

$$\beta_f \approx 9 .$$

Thus, for the tension data, the magnification factor A_1 is

$$A_1 = \left\{ \frac{\beta_{f_{\text{real}}}}{\beta_{f_{A_1}}} \right\}^{\frac{1}{2r}}$$

$$A_1 = \left(\frac{433}{9} \right)^{\frac{1}{10.92}}$$

$$A_1 = 1.4258 ,$$

and for the compression data

$$A_1 = \left(\frac{295}{9} \right)^{\frac{1}{10.92}}$$

$$A_1 = 1.3765$$

These magnification factors were used for the eight lifetime tests discussed in Section 3.6.1.3.

3.7 STATIC AND FATIGUE TEST RESULTS FOR SKIN SPECIMENS

Static and fatigue tests were conducted on $[(0/(\pm 45)_2)_2]_s$ laminate specimens that represented the sandwich skins in the joint specimens. These skin specimens (see Figure 30) were 2.54 cm (1 inch) x 22.86 cm (9 inches) x 20 plies (see Figure 5). They were tested in both tension and compression for four lifetimes with the spectrum described in Section 3.3.

Several specimens were tested in tension to determine the initial static strength of the laminate. Five specimens were then fatigue tested under the tension random load spectrum with a maximum fatigue load of 76 percent of static ultimate. After four lifetimes, the average residual strength of the five specimens was three percent higher than the original static tension strength. Aluminum side support plates were used to stabilize the specimens during the GAG compression load cycles.

Five specimens were also started in testing under a compression fatigue spectrum with a maximum compression load of 76 percent of the static tensile ultimate. After several end grip failures, the maximum spectrum load was reduced to just below the lamina transverse compression failure load for the laminate. At this load level, four lifetimes of fatigue were obtained on five specimens without any failures. Residual compressive strength tests could not be conducted on these specimens because of their very low buckling strength.

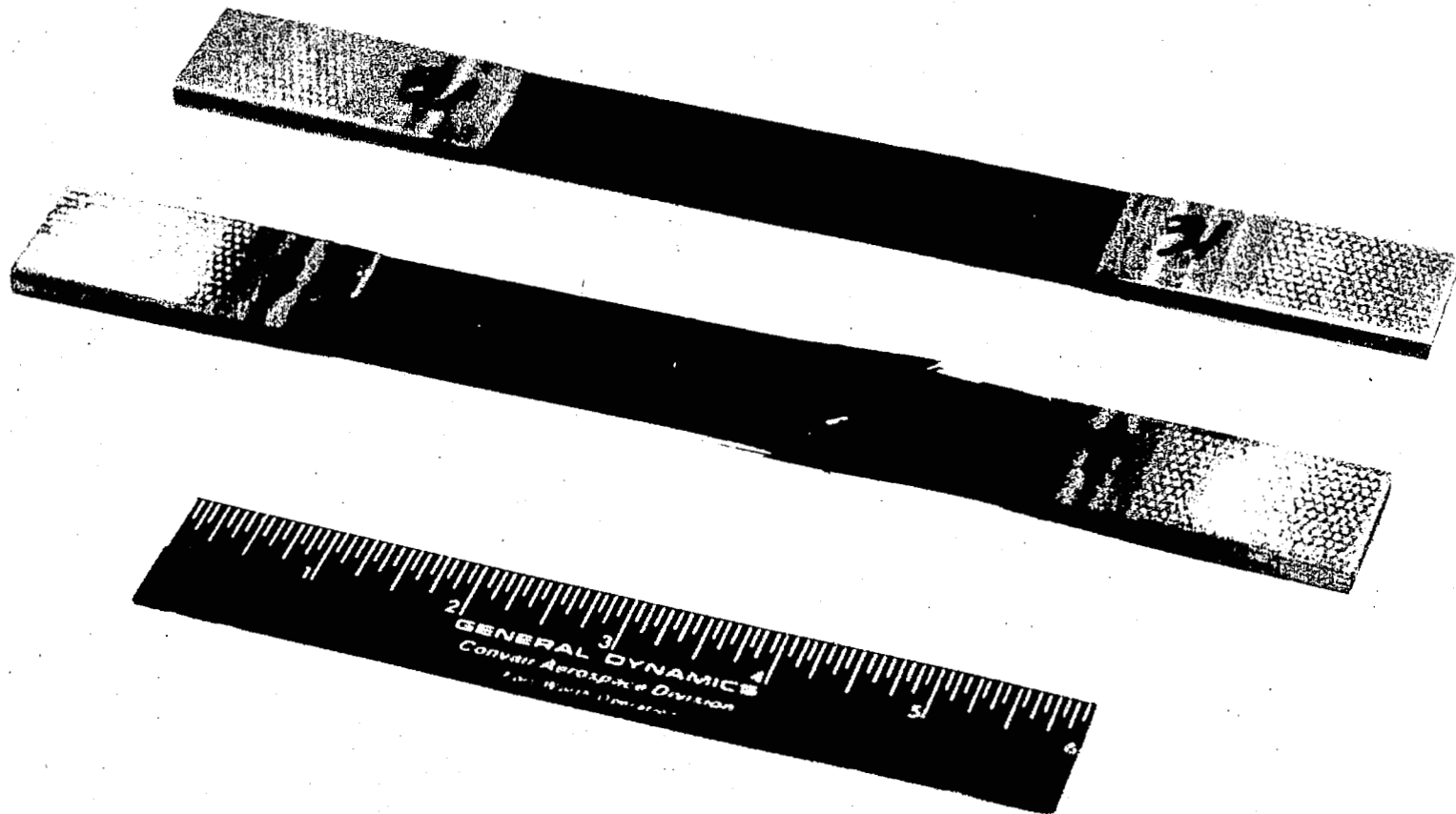


Figure 30 Sandwich Skin Specimens

3.8 DISCUSSIONS

The β_f of the real spectrum was predicted by the wearout model to be 433 lifetimes for the tension splice. Assuming $\alpha_f = 3.36$, the probability of survival at one lifetime is

$$P = \exp \left\{ - \left(\frac{x}{\beta} \right)^{\alpha} \right\}$$

$$P = \exp \left\{ - \frac{1}{433}^{3.36} \right\}$$

$$P = 0.999 \ 999 \ 998 \ 6$$

Now, because this detail (one line of bolts in the total wing splice) would be repeated approximately 60 times in a 1.524m (60 inch) chord wing, the probability of survival for the total splice is

$$P_{\text{splice}} = P_{\text{ele}}^{60}$$

$$P_{\text{splice}} = 0.999 \ 999 \ 916.$$

Thus, the probability of survival of the total wing splice at one lifetime under the real limit load spectrum is quite high.

Another aspect of the test results reveals the relationship between limit and ultimate design stress or load levels. Since the load magnification factor of 1.3636 only raised the peak load to 80.1 kN (18,000 pounds) and did not truncate any loads, let us assume, for the moment, that 80.1 kN (18,000 pounds) is the design limit load level. Now, since the splice was designed to an ultimate load of 100.1 kN (22,500 pounds), the factor of safety relating limit and ultimate load becomes

$$\text{Factor of safety} = \frac{100.1}{80.1}$$

$$\text{Factor of safety} = 1.25.$$

For the 1.3636 magnification factor curves in Figure 28, it may be observed that the splice element has an adequate fatigue life (>10 lifetimes) and at 1.0 lifetime the residual strength

lines are essentially flat. This line of reasoning leads one to the conclusion that a 1.5 factor of safety (a carry-over from metallic design) may be too large for this splice element. A more realistic approach would be to set this overload factor as the load ratio derived from a once per fleet lifetime gust.

The discussion could also be viewed from the overload design procedure outlined in Reference 7. Again referring to the 1.3636 magnification factor curves of Figure 28, the splice specimen has a 0.9 probability of survival of an overload of 93.4 kN (21,000 pounds) or 93 percent of ultimate at 1.0 lifetime. With residual strength data and fatigue lifetime data at two or more levels the entire design procedure as outlined in Reference 7 could be implemented.

The real spectrum (peak load=limit load) tension and compression long term tests have shown that no damage of the specimen occurred during ten lifetimes of testing. The residual strength (based on first nonlinear point) of the tension specimen was reduced however, but still remained considerably above limit load. The compression specimen retained a residual strength above ultimate load.

The eight lifetime magnified tension and compression specimens both failed below the predicted mean life by approximately a factor of two. Since the α_f is 3.36, these tests are well within the expected scatter.

For comparative purposes, an equivalent aluminum splice was designed for static loads only with the same design concept as the graphite tension specimen. Based on 2024-T851 aluminum properties, the static metal design weighed the same as the graphite splice design. A fatigue analysis of the aluminum splice resulted in a predicted lifetime of approximately one for straight bolts and two lifetimes for Taper-Lok fasteners. This compares to the 433 lifetimes predicted by the wearout model (see Section 3.6.3) and the proven ten lifetimes of test in the long term test described in Section 3.6.2 for the graphite splice.

4.0 LARGE PANEL DESIGN AND FABRICATION

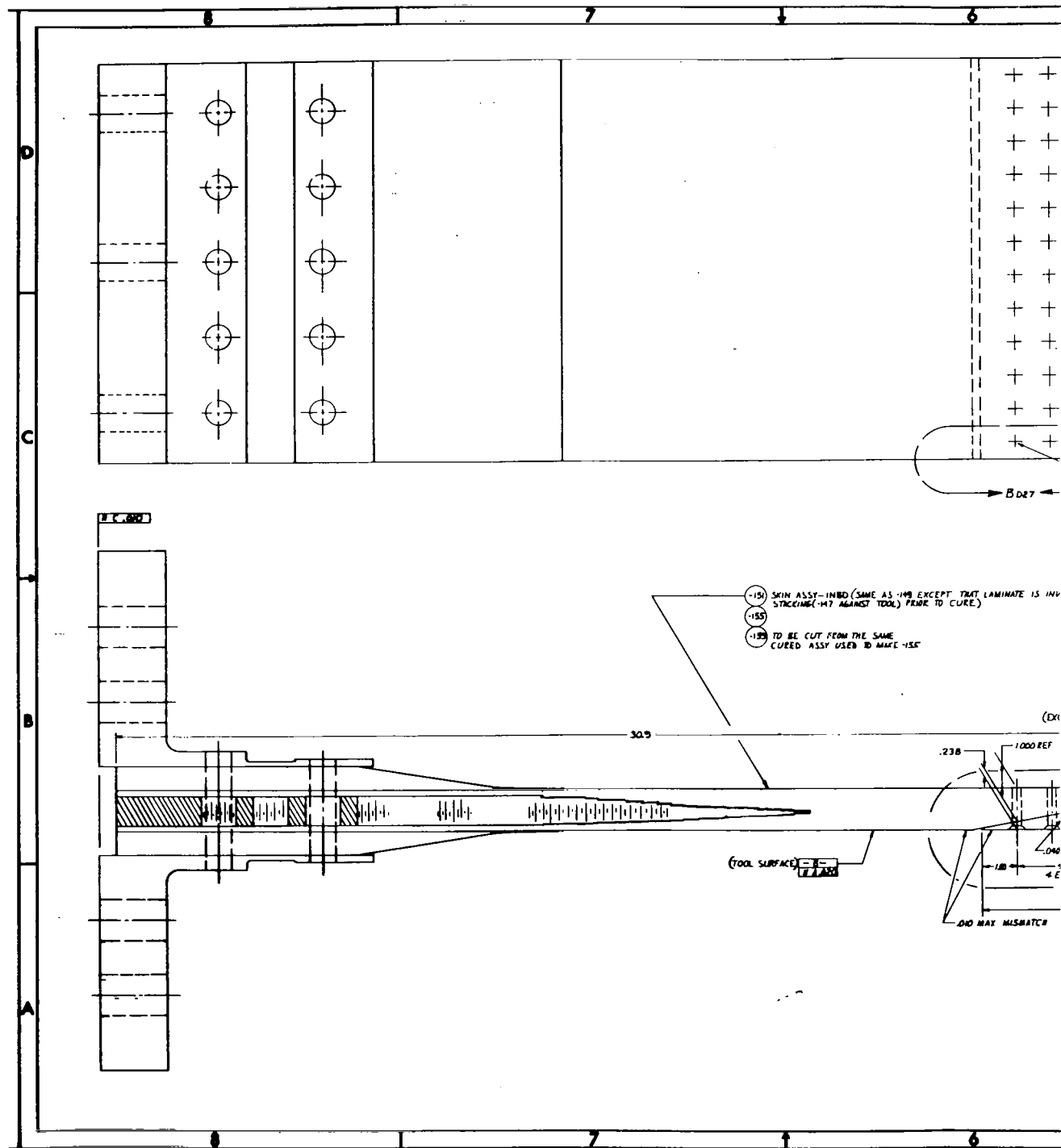
The development test program showed that the design of the splice region provided adequate static strength and fatigue life. Thus, the splice region was not changed for the large panel design. However, changes were made in the transitional region at the beginning of the sandwich construction and in the end grip region in order to eliminate problems that developed in the tests and during fabrication.

4.1 PANEL DESIGN

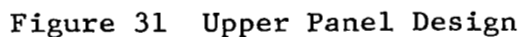
Drawings of the final design for the upper and lower wing skin splice panels are shown in Figures 31 through 34. The specimen length between fiberglass end-tab regions is 0.762 m (30 inches); thus, it is typical of the rib spacing on an advanced transport aircraft. In order to eliminate some of the problems encountered with the bolts used in the earlier development tests, the "Hi-Torque" steel bolts (see Section 3.6.1.1) with a higher heat-treat were specified.

In the development test specimens, the relatively low modulus laminate at the thin end of the splice was extended into the skins of the honeycomb sandwich and into the grip region of the specimen. Since the modulus of this laminate would probably be lower than that for an adjacent panel, some of the ± 45 degree plies were dropped in the outer skin regions and replaced with 0 degree plies in order to obtain an approximately 50 percent 0 and 50 percent ± 45 degree laminate for the sandwich skins. The transition in the skin laminate was made in the same region as the transition from solid laminate to sandwich construction.

The transition from solid laminate to sandwich caused the surface to be uneven in the development test specimens because too many plies were stopped at a step (i.e. as many as 11 plies in 1.524 cm (0.6 inch) long steps). For the large splice panels, only four plies were stopped in 1.016 cm (0.4 inch) long steps. This change lengthened the transition region by approximately 5.08 cm (2.0 inch), and thus reduced the load transfer rate. To further smooth out the surface, a wrap layer consisting of two plies (± 45) of graphite were laid over both sides of the tapered aluminum core. These plies also reduce the stress concentration at the ends of the steps. To prevent end grip failures that



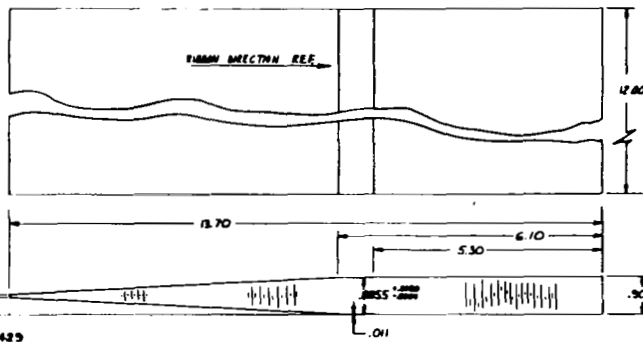




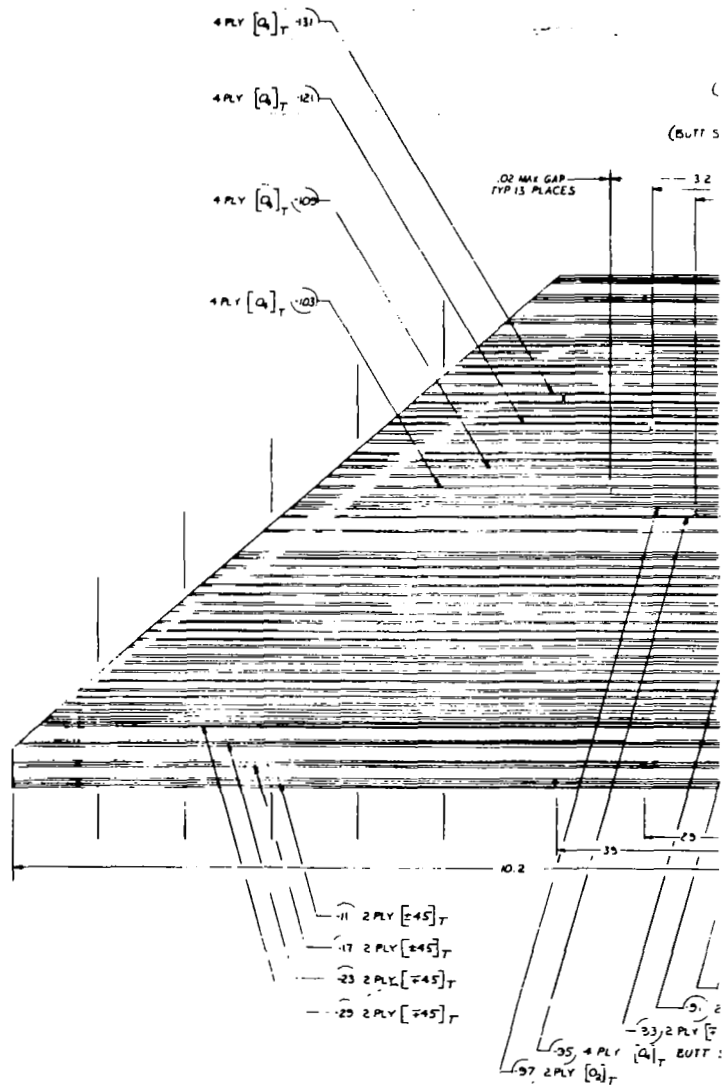


.255
 .250 BM HOLE (S)
 CSK F.S. 100% .507 DIA (.040-.008 REQD AT INTERSECTION WITH .250 BM HOLE)
 (CSK SHALL INSURE FASTENER HEAD FLUSHNESS WITHIN 1.000")
 8T BMS-4-BB (S)
 MS BMS-4-BB (S)
 TORQUE TO 75+25 INCH-POUNDS
 SEE NOTE 1

DETAIL B6 (FOR 3)

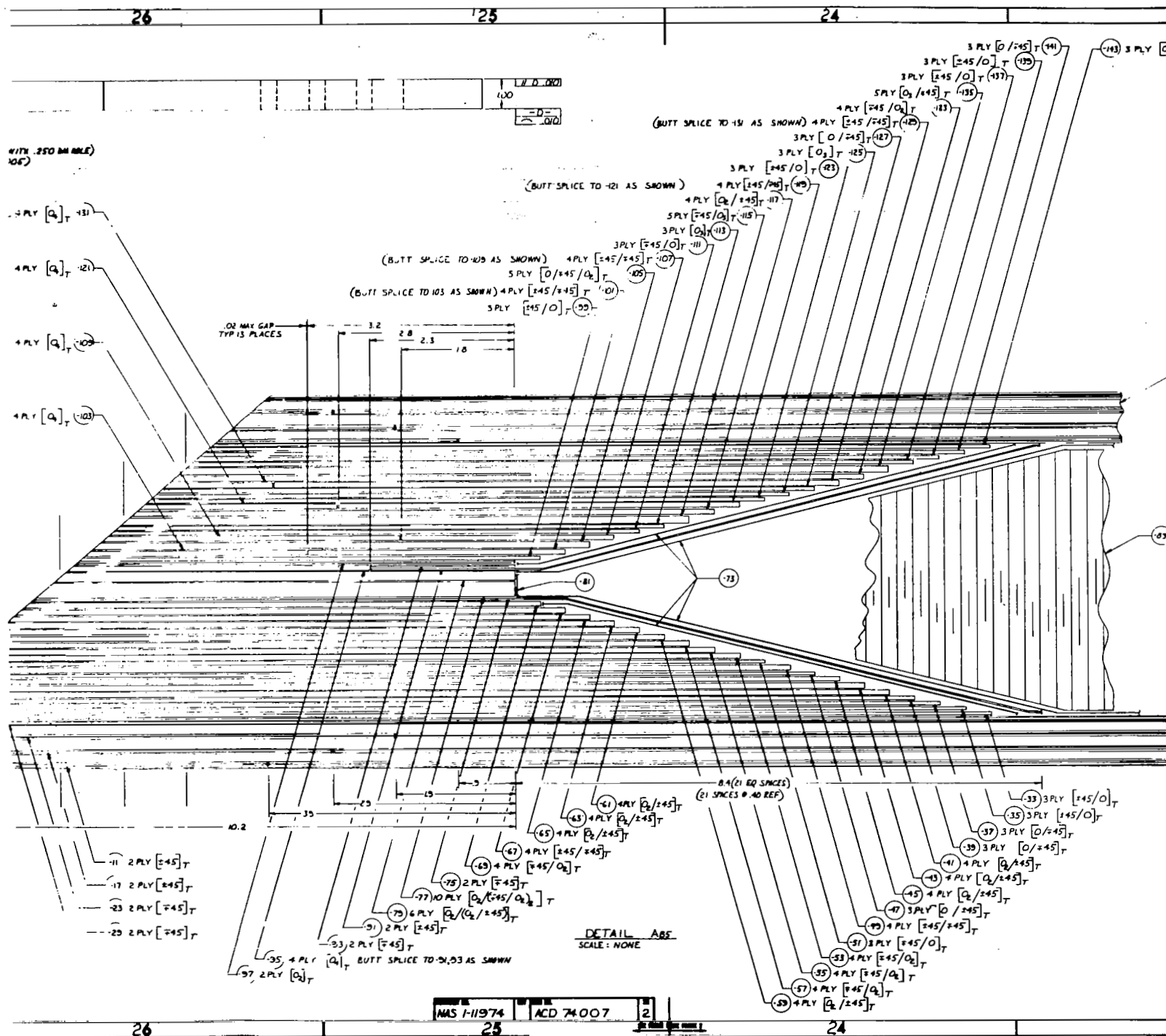


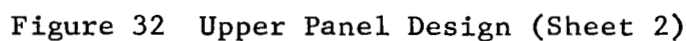
DETAIL B3

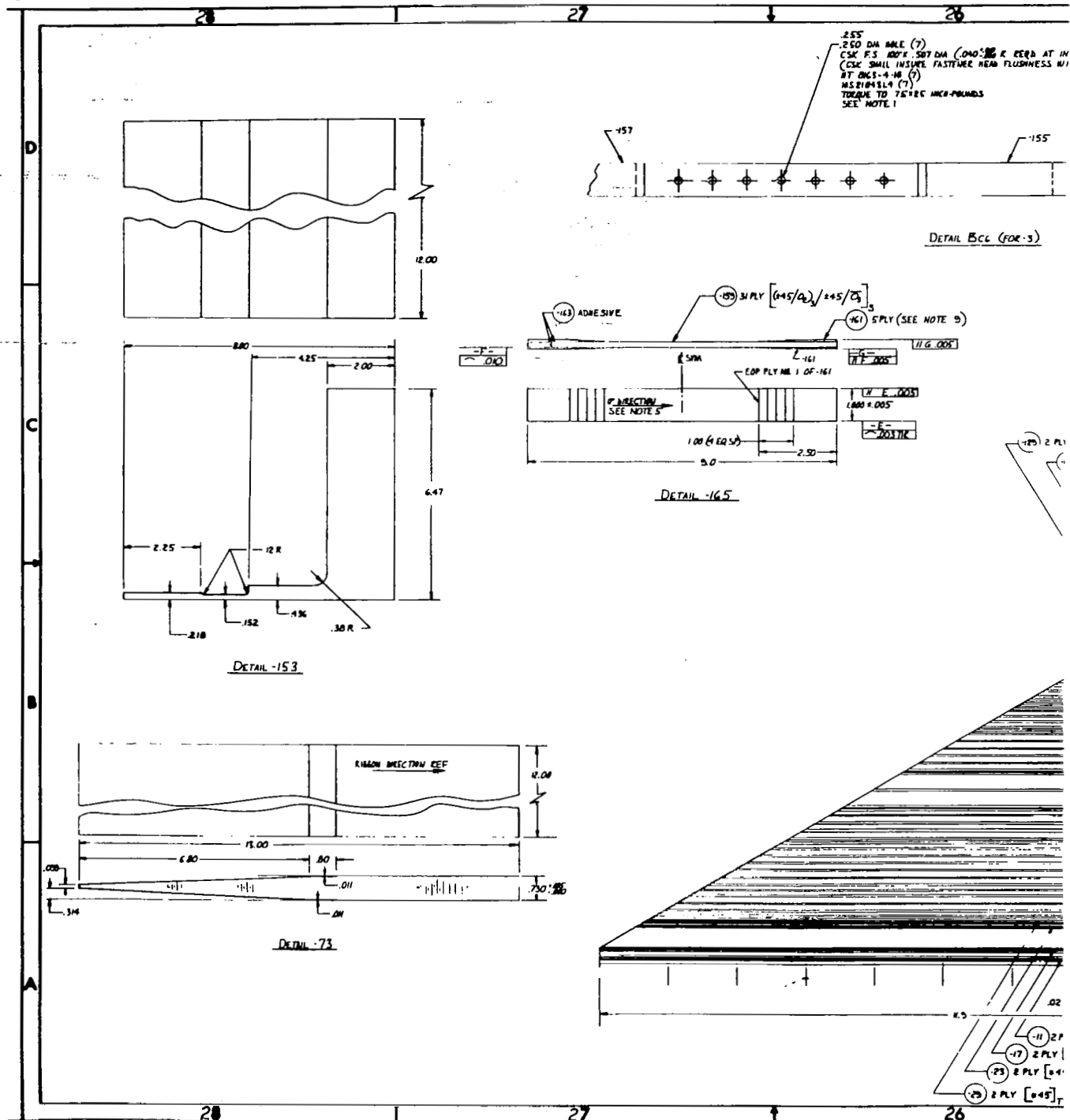


11 2 PLY [45]_T
 17 2 PLY [45]_T
 23 2 PLY [45]_T
 29 2 PLY [45]_T

35 4 PLY [4]_T
 33 2 PLY [4]_T BUTT
 37 2 PLY [4]_T





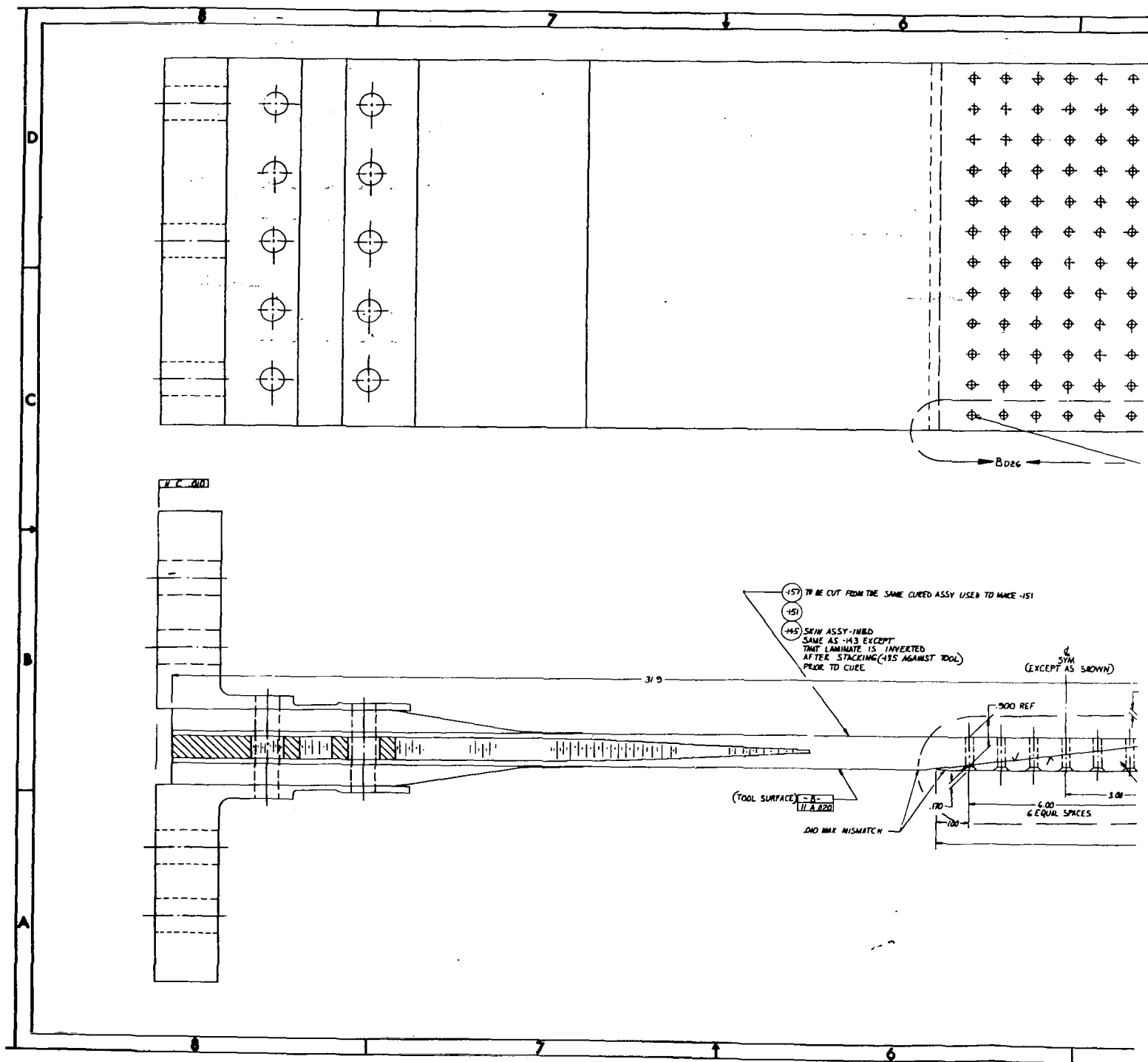


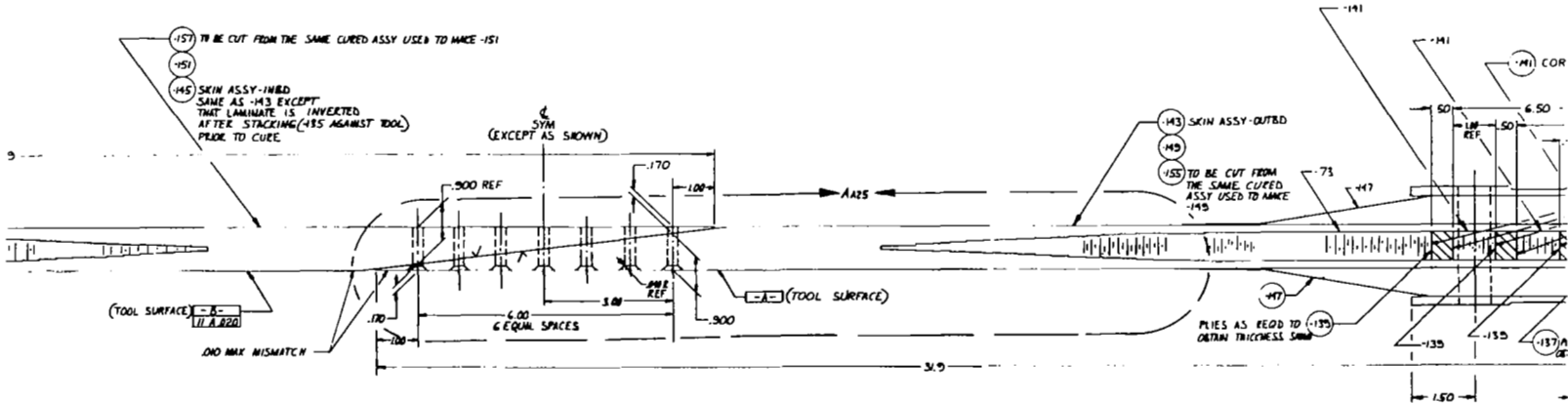
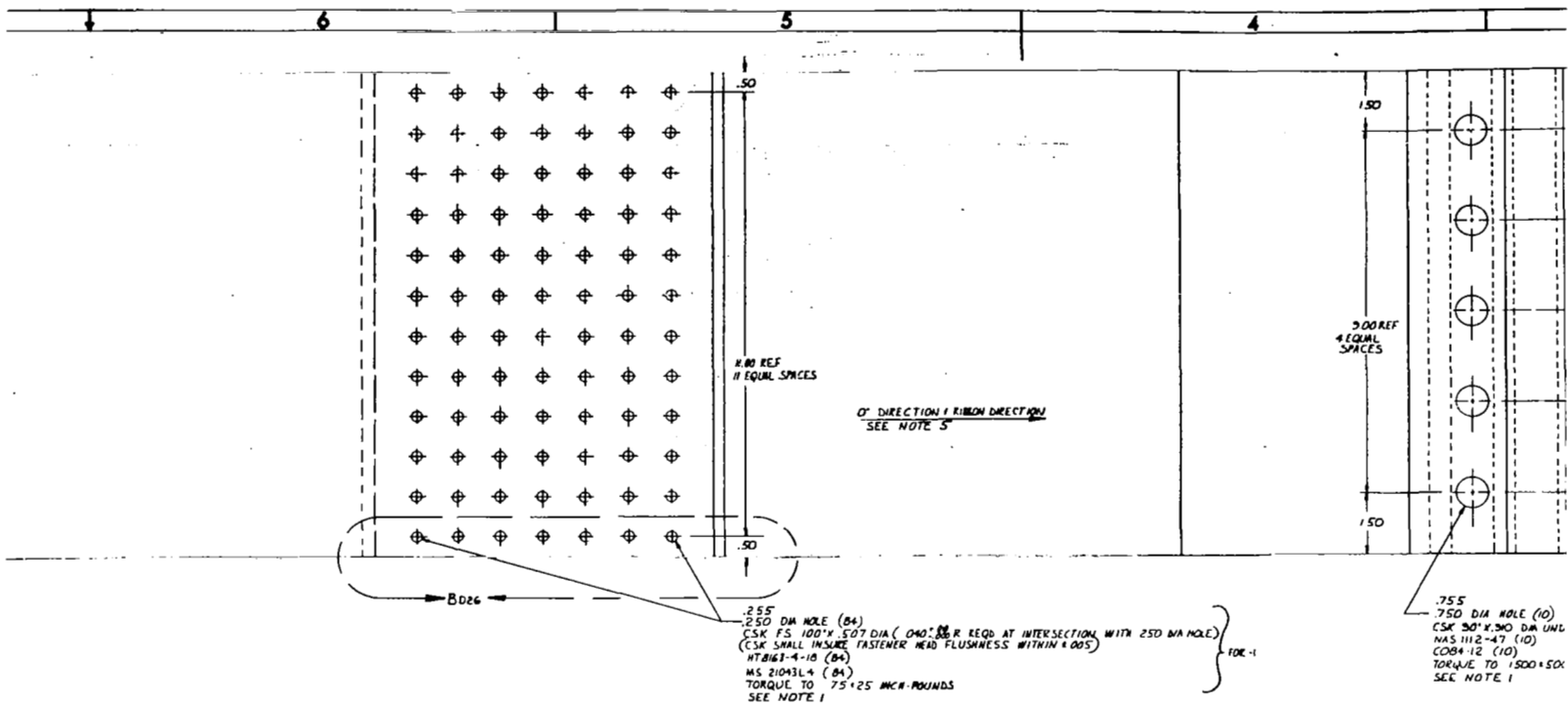


MAS 1-11974

ACD 7400

1





NAS 1-11974

ACD 74008

SEE FIGURE 1

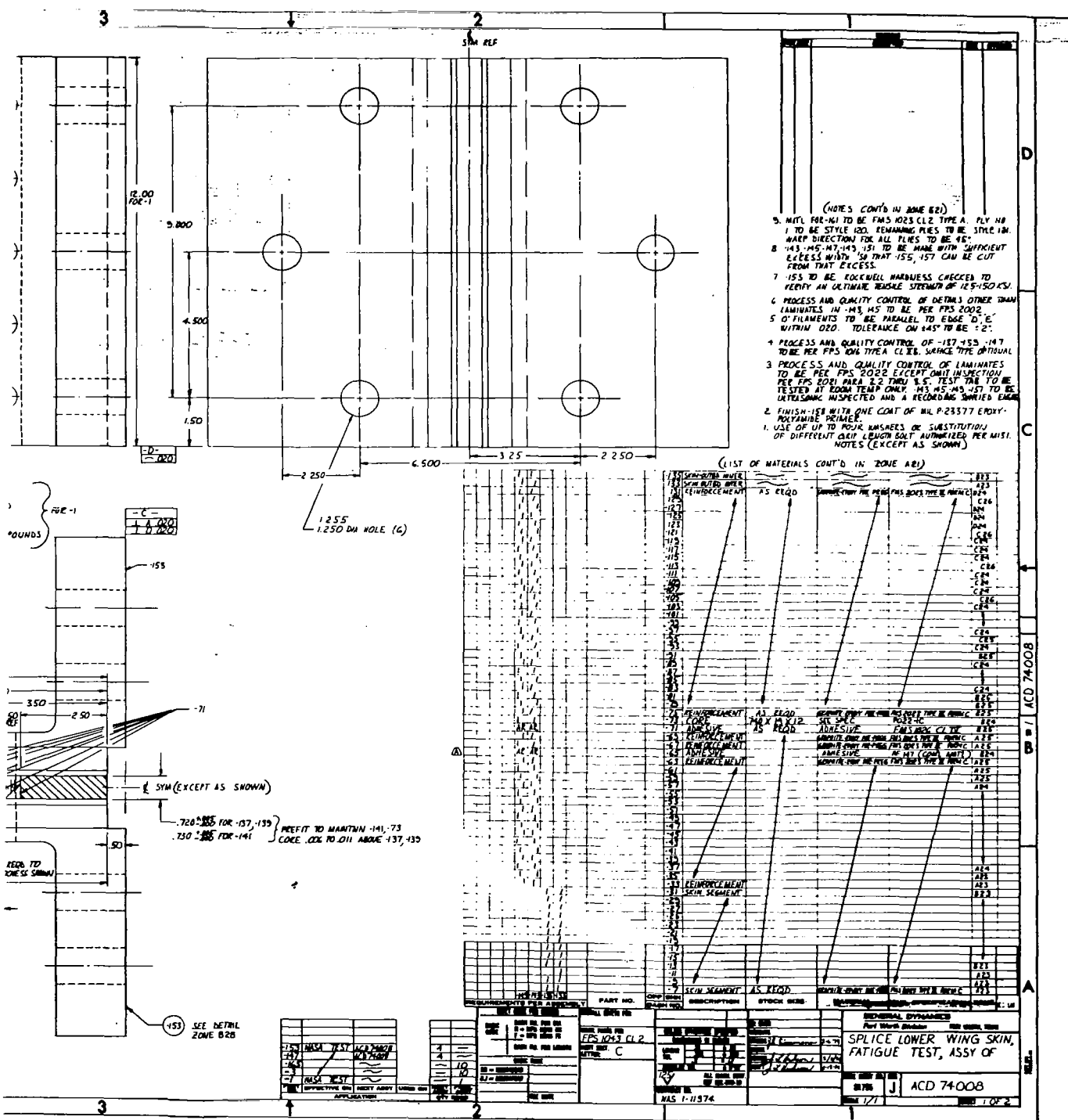


Figure 34 Lower Panel Design (Sheet 2)



Figure 35 Layup Showing Core Details

first occurred in the development tests (Section 3.5.1), the solid fiberglass block was replaced with intermittent strips of fiberglass (see Figure 31).

The steel end angles of Figures 31 and 33 were made to attach the large panels to the NASA test machine. The angles were designed by matching the strain in the steel between the two lines of bolts with the strain in the fiberglass end tabs and the strain in the graphite sandwich faces. A low stress level was used in the steel design to ensure a fatigue life of 10 lifetimes. The static design load for the end grip region was two times limit load.

4.2 PANEL FABRICATION

During the course of the program, the contract was modified to provide NASA-LRC with ten tension and ten compression specimens similar to those of the development test program. These specimens were 2.54 cm (1.0 inch) wide (one row of bolts) and of the same detail geometry as the 30.48 cm (12 inch) wide large panels. To minimize costs, extra wide tension and compression panels were made and then simply cut into 10, 2.54 cm (1.0 inch) specimens and one, 30.48 cm (12 inch) wide specimen each.

Basically the large panels were fabricated similar to the development test specimens. The numerically controlled tape laying machine was used to lay large sheets of multiple ply orientations. These large sheets were then pre-bled to compact the layers and remove most of the excess epoxy that is normally removed during a curing operation. These sheets, which were not cured by the pre-bleeding cycle, were then cut into the required size and number of pieces. Only one end of a panel was assembled and cured at a time rather than both pieces as in the case of the development joint specimens. Figure 35 shows one-half of the graphite sheets, the aluminum core, and the fiberglass strips (pre-cured and machined) in the curing tool. A sheet of adhesive was placed between the core and the ± 45 degree wrap layers on each side. The three white strips along the length of the panel and across the panel at the tapered end of the core are where the core has been filled with a potting compound (see Figure 35). The core was filled with potting compound in these areas to prevent the core from being crushed during final cure. During final cure of the first part of a wide panel, the core crushed and was pushed back along the length of the panel, causing a depression in the outer surface. Potting the core did

not completely eliminate the depression. Figure 36 shows a completed assembly before curing. After curing, pre-cured fiberglass end tabs were bonded to both sides of the panel in the grip area and the panel was cut into specimen and panel widths. Figure 37 shows a 30.48 cm (12.0 inch) wide panel and 10, 2.54 cm (1.0 inch) wide specimens that were cut from one of the wide panels. Next, the sides of the specimens, the scarf surfaces, and the fiberglass end tabs were machined. The specimen halves were then clamped together, the holes were drilled and countersunk, and the bolts were installed. Figure 38 shows a completed tension and compression joint specimen.

The steel angles were next clamped in place on the 30.48 cm (12 inch) wide panels and the two rows of 1.905 cm (0.75 inch) holes drilled through the entire assembly. A facing cut was made across the end of the assembly to ensure that the back of the angles were perpendicular to the surface of the graphite panel. Holes were then drilled in the outstanding legs of the angles for attaching the panels in the NASA test machine. Figure 39 through 42 show views of both sides of the completed tension and compression panels, respectively.

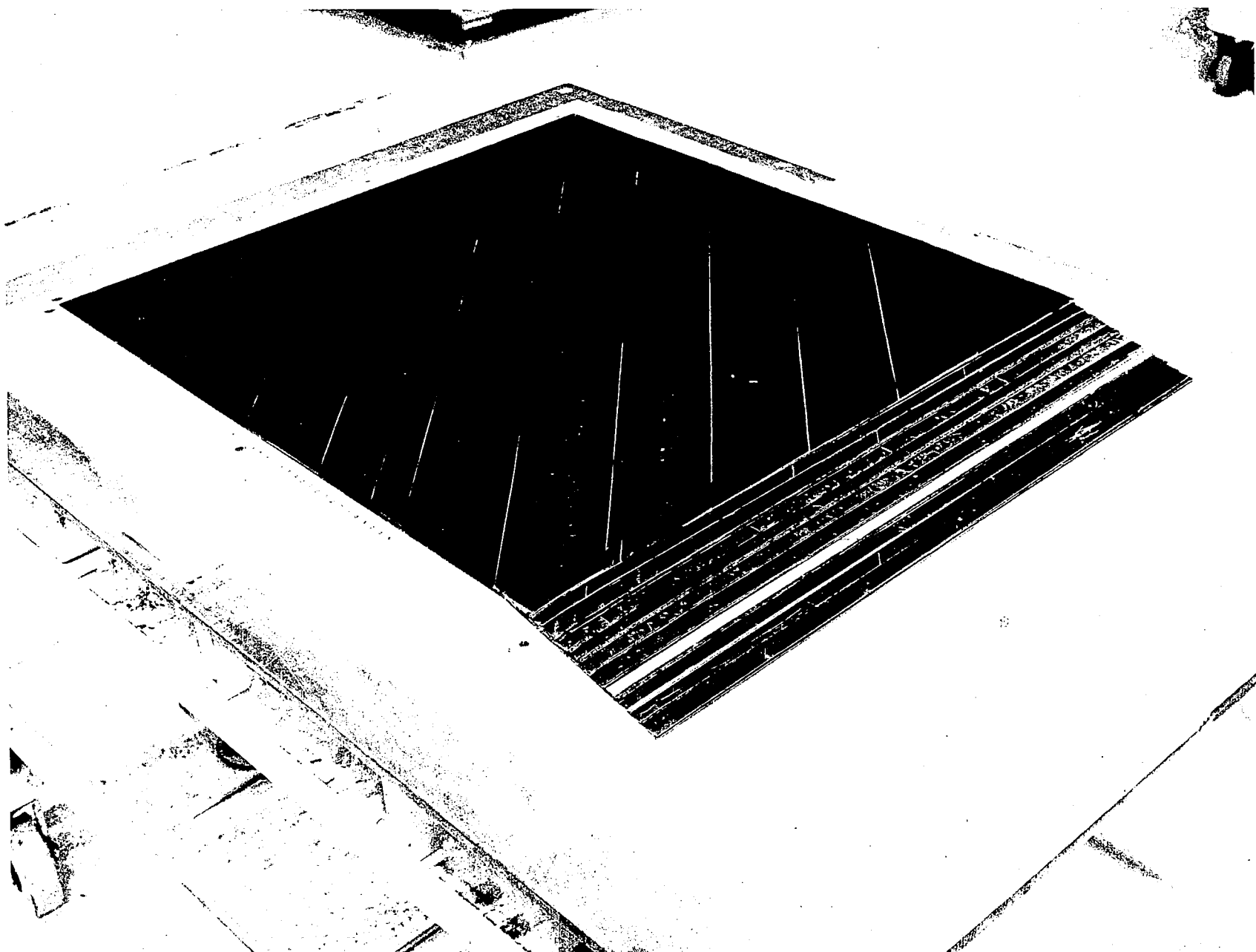


Figure 36 Completed Layup Before Cure

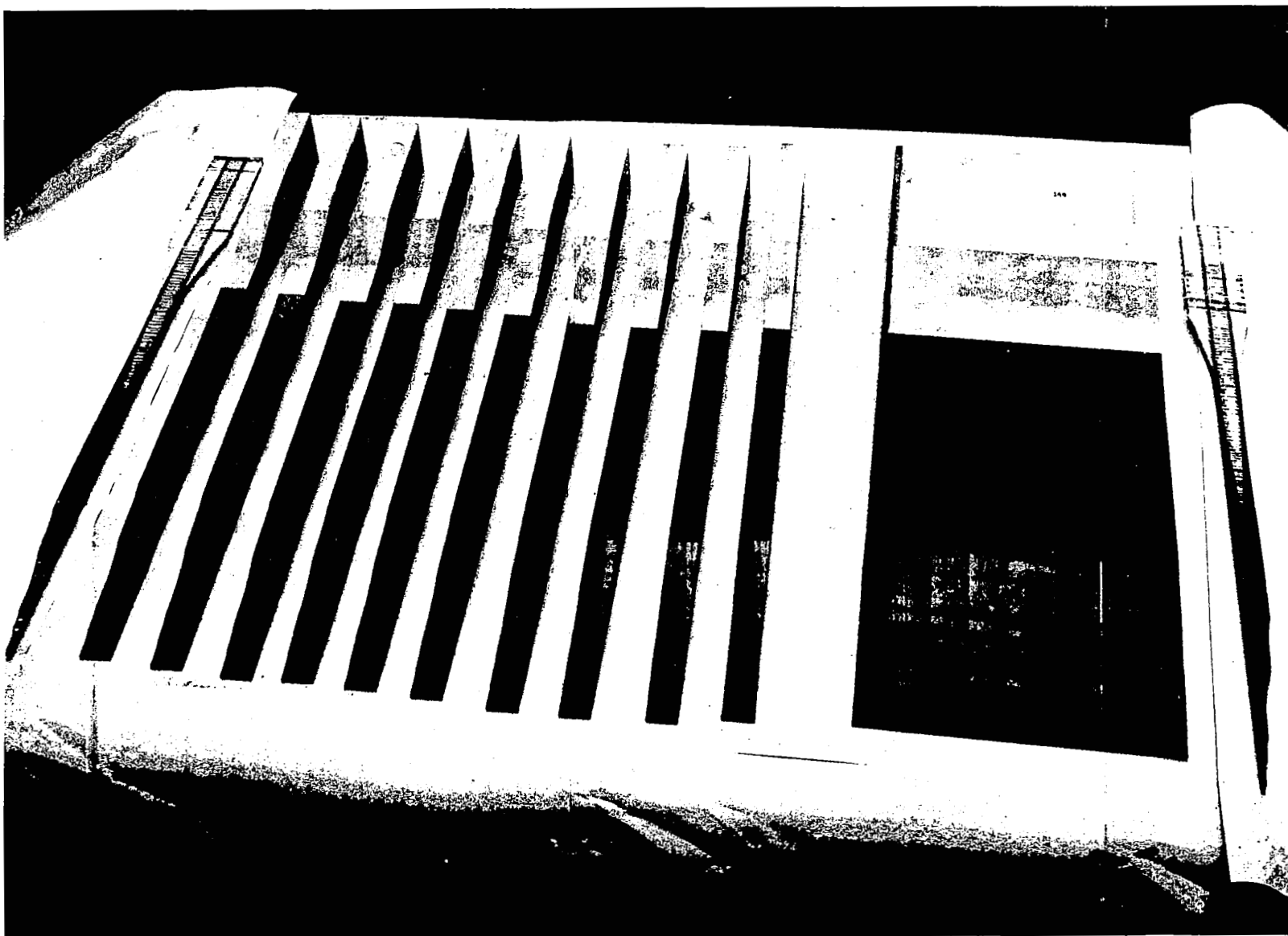


Figure 37 Large Panel and Specimens Cut From Blank



Figure 38 Completed Test Specimens

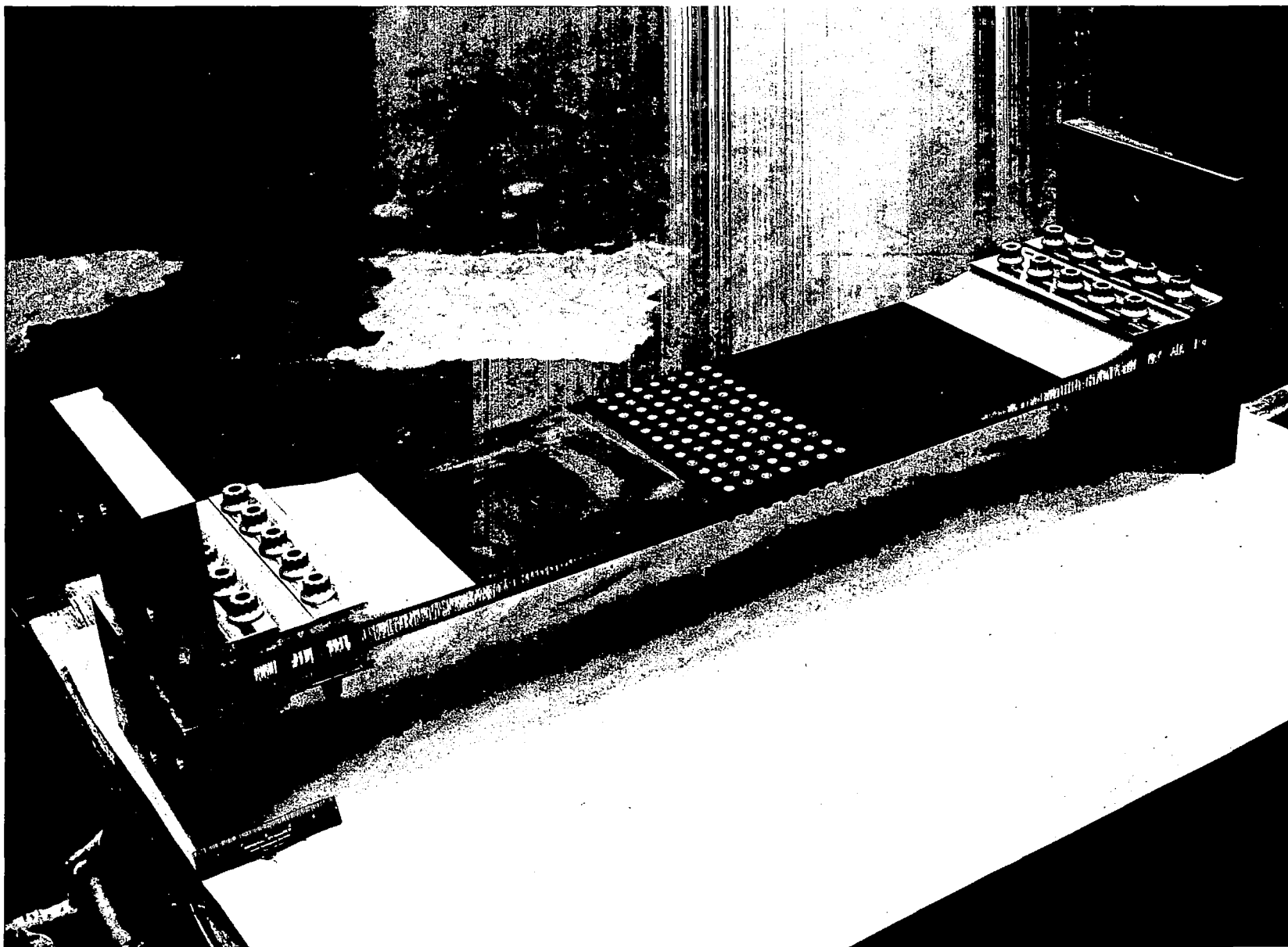


Figure 39 Tension Splice Panel - Outer Surface

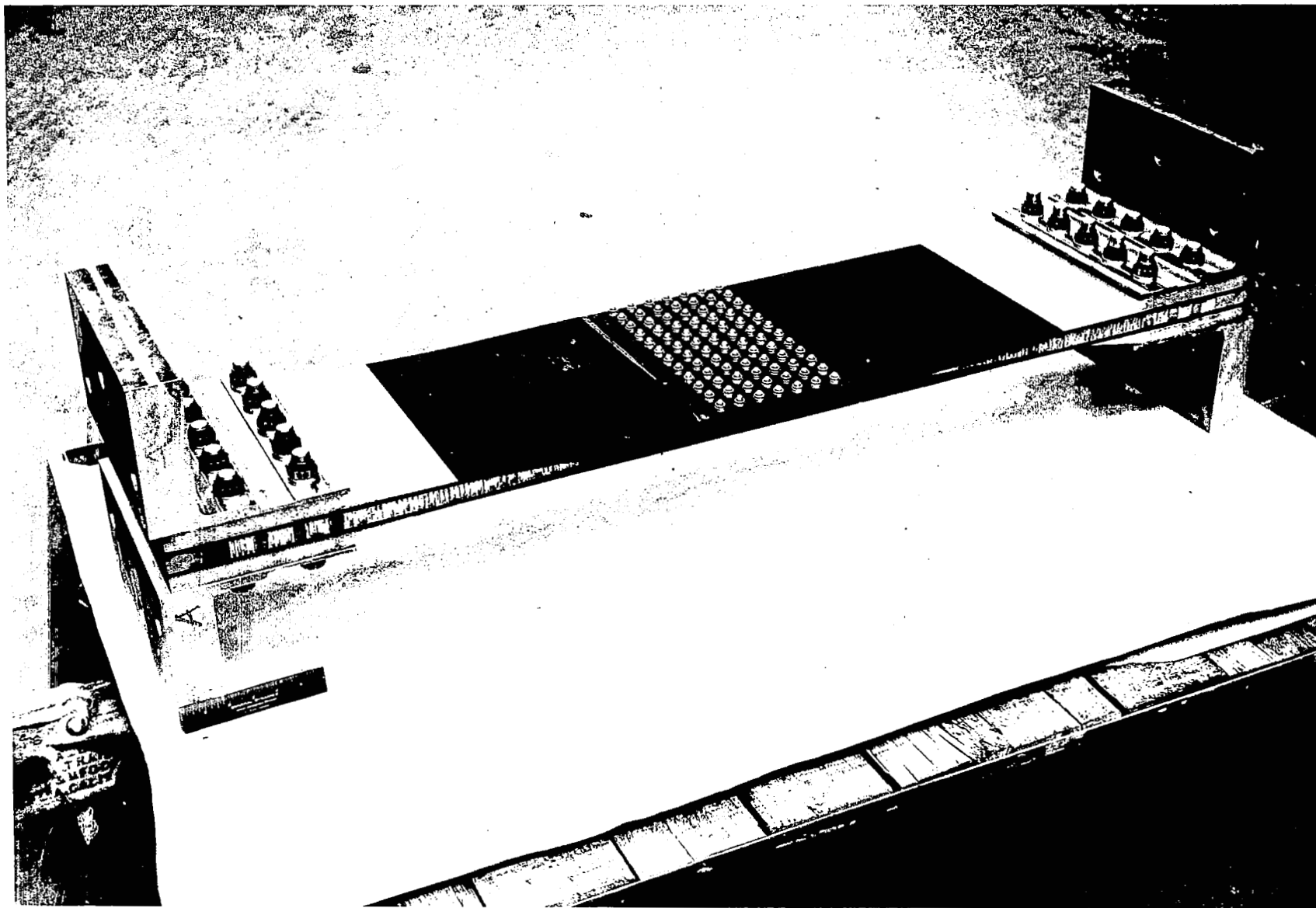


Figure 40 Tension Splice Panel - Inner Surface

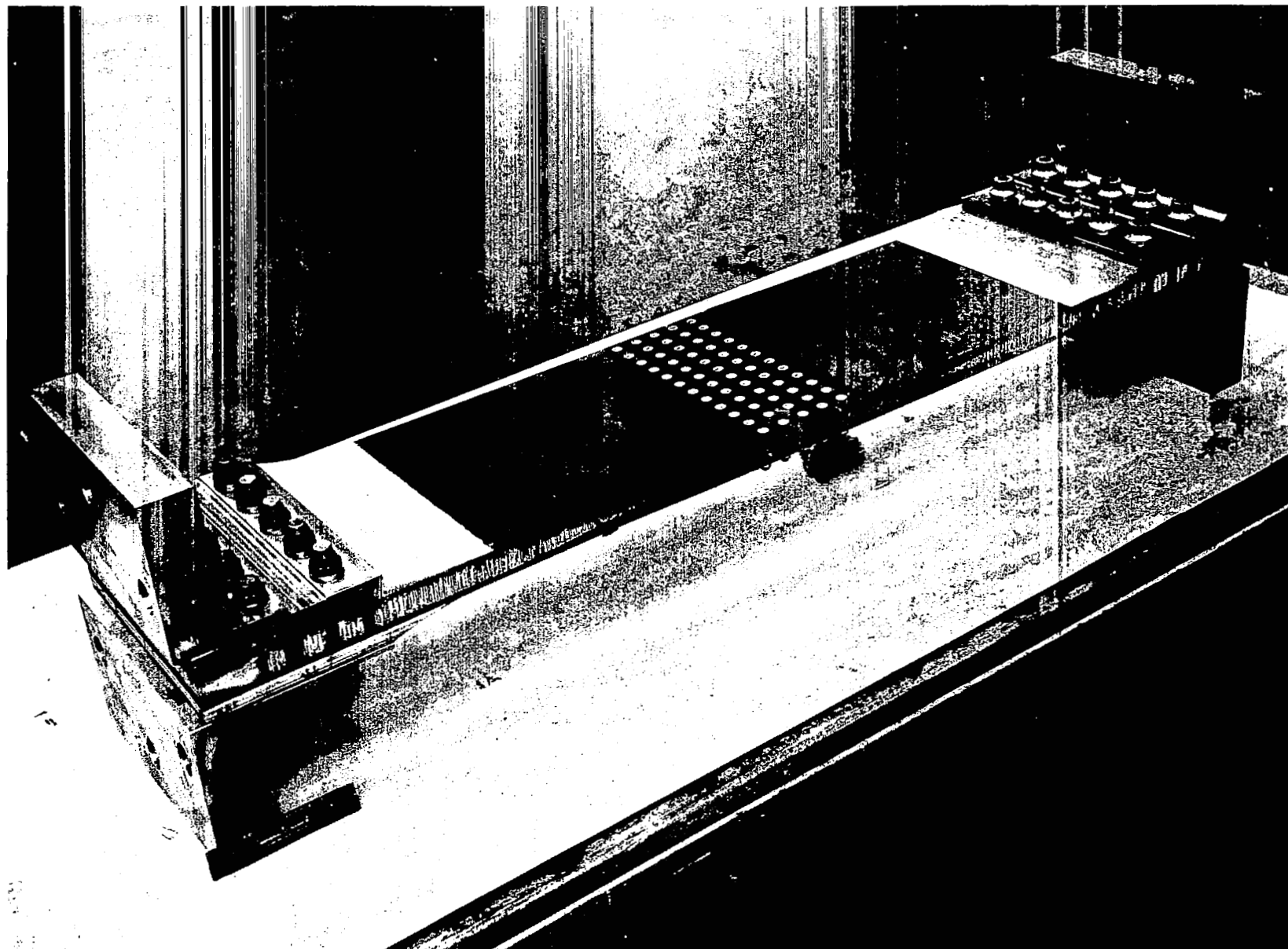


Figure 41 Compression Splice Panel - Outer Surface

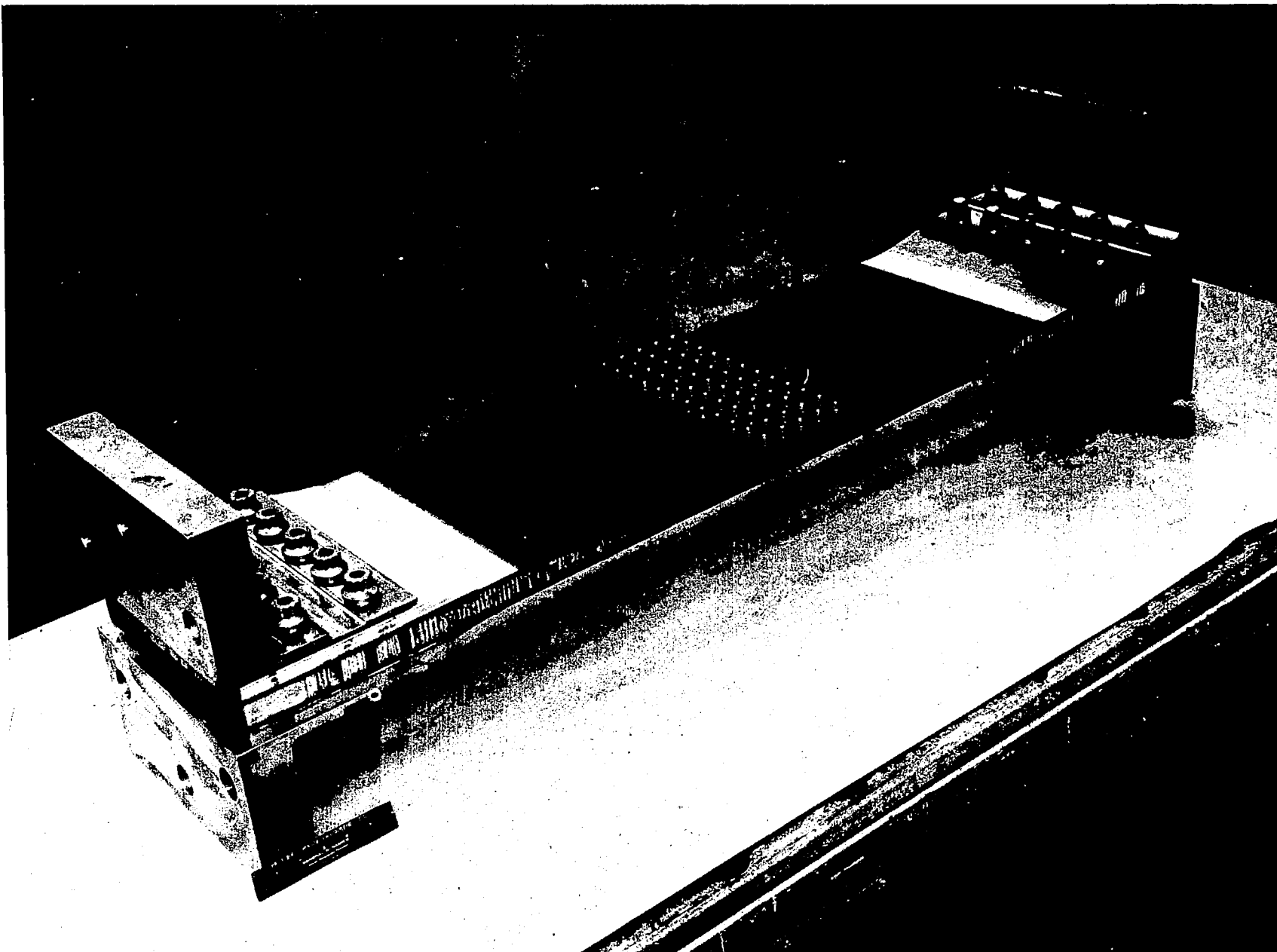


Figure 42 Compression Splice Panel - Inner Surface

5.0 CONCLUSIONS AND RECOMMENDATIONS

The conclusions and recommendations derived from this program are summarized in this section.

5.1 CONCLUSIONS

1. A single scarf bolted joint is a viable design concept for an advanced transport composite-to-composite wing splice.
2. A small number of test specimens can be used to effectively screen design concepts.
3. The small data base can be strengthened by relating it to a large data base from previous testing.
4. The static design of a bolted joint can be based on fracture mechanics concepts.
5. The static design of a bolted joint can give an adequate fatigue life.
6. The wearout model was found to adequately represent the bolted splice fatigue characteristics.
7. The bolted scarf splice concept had a fatigue life in excess of the 60,000 hours required for an advanced transport aircraft.
8. The fabrication of a large composite panel containing a bolted splice is feasible.

5.2 RECOMMENDATIONS

1. The definition of a bearing type fatigue failure should be investigated.
2. The use of proof-loading to censor weak articles and extend the time-to-first failure in a population should be examined.

3. Different types of fasteners for composite materials should be investigated under both static and fatigue loadings.
4. An investigation of accelerated versus real-time fatigue testing should be conducted.
5. The effects of a high humidity environment on static strength and fatigue life of bolted joints should be investigated.
6. New concepts for bolted joints such as softening strips for reducing the stress concentration should be investigated.

6.0 REFERENCES

1. Waddoups, M. E., Eisenmann, J. R., and Kaminski, B. E., "Macroscopic Fracture Mechanics of Advanced Composite Materials," Journal of Composite Materials, Volume 5, October 1971.
2. Manning, S. D., and Lemon, G. H., "Evaluation," Study of Structural Criteria for Composite Airframes, Volume I, April 1973.
3. Wilkins, D. J., Wolff, R. V., Shinozuka, M., and Cox, E.F., "Realism in Fatigue Testing: The Effect of Flight-by-Flight Thermal and Random Load Histories on Composite Bonded Joints," Presented to ASTM Symposium on Fatigue of Composite Materials, December 1973. (Will appear in an ASTM STP)
4. Chang, F. H., Couchman, J. C., Eisenmann, J. R., and Yee, B. G. W., "Non-destructive Test Technique for the Detection of Damage Near Stress Concentrations in Advanced Composite Laminates," Presented at the Composite Reliability Conference, Las Vegas, April 1974.
5. Halpin, J. C., Waddoups, M. E., and Johnson, T. A., "Kinetic Fracture Models and Structural Reliability," International Journal of Fracture Mechanics, Volume 8, 1972, pp. 465-468.
6. Halpin, J. C., Jerina, K. L., and Johnston, T. A., Characterization of Composites for the Purpose of Reliability Evaluation, AFML-TR-72-289, December 1972. (Also appears in ASTM STP 521)
7. Eisenmann, J. R., Kaminski, B. E., Reed, D. L., and Wilkins, D. J., "Toward Reliable Composites: An Examination of Design Methodology," Journal of Composite Materials, Volume 7, No. 3., July 1973.